region between the metal atoms, by overlap between the two metals. The resulting dipole moment is along the positive y-axis. The magnetically allowed transition ($7b_{2u} \rightarrow 5a_u$, Figure 9b) involves a counterclockwise charge rotation about the y-axis and a consequent dipole moment along positive y.

For the 600-nm CD transition, the electric and magnetic moments are in opposite directions, while for the 450-nm band the two moments are parallel. Although the relationships of electric and magnetic moments are counterposed for the two bands, so also are the perturbation coefficients for excited-state mixing in the two cases. The denominator in eq 4a is different in sign for the two transitions in the absence of a very unlikely, major rearrangement of lower lying energy levels upon activation of any of the transitions under consideration. We can see from Figure 7 that the 600-nm CD band arises from mixing of a higher energy magnetic excited state into a lower lying electronic excited state. The denominator in eq 4a for this transition is, therefore, negative. As Figure 7 shows, the opposite is true for the 450-nm CD band.

With our assignments of the CD bands, then, the bands at 600 and 450 nm *must* have the same sign. We observe this for both compounds **1** and **2**, and we have observed the same effect in some half-dozen other chiral compounds with the same $Rh_2(O_{eq})_8(O_{ax})_2$ chromophore (to be reported elsewhere). This gives further support to the assignments as well as to the applicability of the one-electron, static-coupling mechanism to these compounds.

(c) **Assignment of the CD Band at 500 nm.** We have already discussed the fact that mixing of a magnetically accessible excited state into an electronically accessible state can be accompanied by a reverse mixing which gives rise to a CD effect with a sign opposite to that of the first. In compounds **1** and **2** we observe, in the area between the 600- and 450-nm bands, a third CD effect, opposite in sign to the first two. As Figure 7 shows, the relevant magnetic transitions are near each other in the region between the electronic transitions. We assign the 500-nm band to an overlap of these two magnetically allowed transitions, which are activated in the CD by the reverse-mixing process. There is no question about the nature of the 500-nm band; it does not appear in the electronic spectrum, and, therefore, it is a magnetically allowed transition.

While there is little doubt that the assigned transitions are active in this region, it is also possible that a magnetically allowed $\delta(Rh-Rh) \rightarrow \sigma^*(Rh-O)$ transition is also active (transition E in Figure 7). This could affect the relative intensities of the three CD peaks; we are currently investigating this and other features of the CD spectra of chiral dirhodium tetracarboxylates.

Acknowledgment. We are grateful to the National Science Foundation for support. We also thank Professor Graham Palmer of Rice University for very graciously allowing us to use his JASCO (J500-C) CD/ORD spectrometer to check and confirm our observations.

Registry No. 1, 100019-76-9; **2**, 100019-77-0.

Supplementary Material Available: Full tables of bond distances and angles, anisotropic displacement parameters, and observed and calculated structure factors for the crystal structures of **1** and **2** (91 pages). See any current masthead page for ordering information.

High-Valent Iron Porphyrins: Synthesis, X-ray Structures, π-Cation Radical Formulation, and Notable Magnetic Properties of Chloro(*meso*-tetraphenylporphinato)iron(III) Hexachloroantimonate and Bis(perchlorato)(*meso*-tetraphenylporphinato)iron(III)

Pierre Gans,[1] Georges Buisson,[2] Emile Duée,[2] Jean-Claude Marchon,*[1] Brian S. Erler,[3] William F. Scholz,[3] and Christopher A. Reed*[3]

Contribution from the Département de Recherche Fondamentale, Centre d'Études Nucléaires de Grenoble, 85X, 38041 Grenoble, France, and Department of Chemistry, University of Southern California, Los Angeles, California 90089-1062. *Received July 22, 1985*

Abstract: The collective evidence from electronic, infrared, Mössbauer, and ^1H NMR spectroscopies, from X-ray crystal structure determinations, from electrochemical studies, and from magnetic susceptibility data provides unambiguous evidence that $[FeCl(TPP\cdot)]^+$ and $Fe(OClO_3)_2(TPP\cdot)$ (TPP = *meso*-tetraphenylporphinate) are iron(III) porphyrin π-cation radical species rather than iron(IV) complexes. The distinction is real, not semantic, and greatly affects the physical and chemical properties of high-valent iron porphyrins. Strong antiferromagnetic coupling ($|-2J| \gtrsim 500$ cm^{-1}) of the $S = {}^5/_2$ iron atom with the $S = {}^1/_2$ porphyrin radical leads to an overall $S = 2$ state for $[FeCl(TPP\cdot)][SbCl_6]$ (**1**) ($\mu_{eff}^{300K} = 4.8\ \mu_B$). By contrast, ferromagnetic coupling ($2J \simeq +80$ cm^{-1}) in $Fe(OClO_3)_2(TPP\cdot)$ (**2**) leads to an $S = 3$ ground state ($\mu_{eff}^{300K} = 6.5\ \mu_B$). X-ray crystal structure determinations of the *p*-tolyl analogue of **1**, $[FeCl(TpTP\cdot)][SbCl_6]\cdot 2C_2H_2Cl_4$ (**3**), and of **2** provide an orbital symmetry rationale for this sharply contrasting magnetic behavior and give new insight into the magnetic coupling of a metal to a porphyrin cation radical. An explanation is offered for the insignificant coupling ($J \sim -2$ cm^{-1}) in compound I of horseradish peroxidase. Crystal data for **3**: monoclinic, space group $P2_1/c$, $Z = 4$, $a = 10.98$ (1) Å, $b = 22.57$ (1) Å, $c = 23.65$ (1) Å, $\beta = 97.73$ (5)° at −140 °C, $R = 0.088$, $R_w = 0.097$, Fe-N_{av} = 2.07 (1) Å, Fe-Cl = 2.168 (5) Å. Crystal data for **2**: monoclinic, space group $P2_1/c$, $Z = 2$, $a = 12.132$ (1) Å, $b = 14.622$ (2) Å, $c = 13.153$ (1) Å, $\beta = 127.84$ (1)° at 25 °C, $R = 0.116$, $R_w = 0.130$, Fe-N_{av} = 2.045 (10) Å, Fe-O = 2.13 (1) Å.

High-valent iron porphyrin complexes have been challenging target molecules for synthetic inorganic chemists during the last decade. The term "high-valent" is used to refer to iron porphyrin complexes more oxidized than the iron(III) oxidation state, the stable state under aerobic conditions. The intense interest in these compounds stems from the demonstrated or proposed involvement of species of this type in various biological processes mediated by peroxidase and catalase,[4-6] by cytochrome P-450,[7] and in model

(1) Laboratoires de Chimie, Département de Recherche Fondamentale.
(2) Service de Physique, Département de Recherche Fondamentale.
(3) University of Southern California.

0002-7863/86/1508-1223$01.50/0

systems.[8] Three distinct methods have been used so far to generate high-valent iron porphyrins: (1) one-electron oxidation of five-coordinate iron(III) porphyrins by iodine–silver perchlorate or by controlled-potential electrochemistry,[9-11] (2) two-electron oxidation of iron(III) porphyrins by iodosylbenzene or *m*-chloroperoxybenzoic acid,[12,13] and (3) homolysis of the O–O bond in μ-peroxo iron(III) porphyrin dimers.[14,15] New chemical methods for producing singly oxidized species are the subject of the present report.

Of major concern has been the correct formulation of these oxidized species, While the alternative possibilities of metal-centered oxidation or porphyrin-centered oxidation have long been recognized, it is only very recently that discerning criteria have been adequately developed, It was first reported by Wolberg and Manassen[9] in 1970 that five-coordinate (tetraphenylporphyrinato)iron(III) complexes FeX(TPP),[16] in which X is a univalent monodentate anionic ligand, can be oxidized electrochemically to one-electron oxidation products $[FeX(TPP)]^+$. A low-spin iron(III) porphyrin π-radical formulation was given to the species. In independent work, Felton, Dolphin, Fajer, and co-workers[10] confirmed the electrochemical synthesis, but they proposed a high-spin iron(IV) electronic ground state for $[FeCl(TPP)]^+$ on the basis of UV–vis and ^1H NMR spectroscopy. Recent work by Goff and co-workers,[11] and from our own laboratories,[17-19] has challenged these conclusions and has required a reinterpretation of the earlier work.[8b] It turns out that the singly oxidized species derived from FeCl(TPP) and FeCl(OEP) are better formulated as high-spin iron(III) porphyrin π-cation radicals rather than iron(IV) complexes.

Our approach to this problem has been to work out improved synthetic methods that would allow high-valent iron porphyrin complexes to be isolated in analytically pure form for definitive characterization. Mössbauer spectroscopic data and accurate crystal structural information were thought to be particularly desirable to resolve the ambiguity about the precise nature and formulation of these compounds. In this paper we fully report the isolation and characterization of two oxidized iron(III) porphyrin complexes, $[FeCl(TPP)][SbCl_6]$ (**1**) and $Fe(OClO_3)_2(TPP)$ (**2**), Some aspects of this work have been previously communicated.[17-19]

Upon establishing that porphyrin ring oxidation is occurring in **1** and **2** it became of interest to explore how the unpaired electrons of the iron atom interact with the π-cation radical ligand. There is very little understanding of such interactions in metalloporphyrin π-radicals or in hemoproteins. The adjacent $S = 1$ iron(IV) and $S = {}^1/_2$ porphyrin radical spin states of compound I of horseradish peroxidase (HRP I) are often loosely referred to as an $S = {}^3/_2$ state when in fact they behave as almost independent spin states.[5b,20] By contrast, we find that complexes **1** and **2** both have strong intramolecular magnetic interactions. It is intriguing, however, that the interaction is *antiferro*magnetic in $[FeCl(TPP\cdot)]^+$ but *ferro*magnetic in $Fe(OClO_3)_2(TPP\cdot)$. A structurally based explanation is offered which takes into account the symmetries of the magnetic orbitals.

Experimental Section

Physical Measurements. Electronic spectra were recorded on a Beckman Acta MVI spectrometer or a Hewlett-Packard 8450A UV/vis spectrophotometer. IR spectra were obtained on a Perkin-Elmer 281 spectrometer. Proton NMR spectra were run at 250 MHz on a Cameca 250 spectrometer in the Fourier transform mode (200–1000 transients). EPR spectra were recorded on a Varian E 04 spectrometer operating at a frequency of ca. 9 GHz.

Electrochemical measurements were done with a three-electrode potentiostatic system. The working electrode was a Tacussel rotating platinum disk (600 rpm) for steady-state voltammetry. The reference electrode was a KCl saturated calomel electrode (Tacussel RDJ/ClO) separated from the bulk solution by a salt bridge (10^{-1} M tetrabutylammonium perchlorate in acetonitrile). Voltammograms were recorded with a Tacussel PRT 500 LC potentiostat driven by a Tacussel GSTP programmer. Large-scale electrolyses and coulometric measurements were done with a Tacussel ASA 100 potentiostat and a Tacussel IG 3 coulometer. Potentials were measured with ferrocene as an internal standard[21] but are quoted vs. SCE by adding 0.38 V.

Mössbauer spectra were obtained by using a constant acceleration electromechanical drive system together with a multichannel analyzer for collecting and storing the data. ^{57}Co in rhodium was used at room temperature as the source. The velocity calibrations were done with a thin iron metal absorber, and all the isomer shift data given in this paper refer to the symmetry center of the iron metal Mössbauer sextuplet at 300 K. The samples were composed of a microcrystalline powder pressed between two polyethylene foils. The mass of the samples (100–200 mg) corresponds to an iron concentration of 10–20 mg/cm^2.

Spectra were analyzed by a least-squares fit program with two independent Lorentzian lines. Experimental values of the Mössbauer parameters δ and ΔE_Q were obtained from these fits.

Materials. Dichloromethane was either refluxed over calcium hydride under argon for 24 h before use or stored on a column of neutral alumina for a week. 1,1,2,2-Tetrachloroethane was used as recieved. Hexane was distilled from calcium hydride and stored over molecular sieves (Linde, 3 Å). FeCl(TPP) and related species were prepared by the Adler method,[22] and $(FeTPP)_2O$ was made by ligand exchange.[23] $Fe(OClO_3)TPP$ was synthesized as previously described.[24] Thianthrene (Aldrich),

(4) Dunford, H. B.; Stillman, J. S. *Coord. Chem. Rev.* **1976**, *19*, 187–251. Dunford, H. B. *Adv. Inorg. Biochem.* **1982**, *4*, 41.

(5) (a) Hewson, W. D.; Hager, L. P. "The Porphyrins", Dolphin, D., Ed.; Academic Press: New York, 1979; Vol. 7, pp 295–332. (b) Schulz, C. E.; Rutter, R.; Sage, J. T.; Debrunner, P. G.; Hager, L. P. *Biochemistry* **1984**, *23*, 4743–4754.

(6) (a) Dunford, H. B.; Araiso, T.; Job, D.; Ricard, J.; Rutter, R.; Hager, L. P.; Wever, R.; Kast, W. M.; Boelens, R.; Ellfolk, N.; Ronnberg, M. "The Biological Chemistry of Iron"; Dunford, H. B.; Dolphin, D.; Raymond, K. N.; Sieker, L., Eds.; D. Reidel: Dordrecht, 1982; pp 337–355. (b) Hoffman, B. M. Ibid. pp 391–403. (c) Jones, P. Ibid. pp 427–438.

(7) (a) Groves, J. T. "Metal Ion Activation of Dioxygen"; Spiro, T. G., Ed.; Wiley Interscience: New York, 1980; pp 125–162. (b) Chang, C. K.; Dolphin, D. "Bioorganic Chemistry"; Van Tamelen, E. E., Ed.; Academic Press: New York, 1978; Vol. 4, pp 37–80.

(8) (a) Dolphin, D.; ref 6, pp 283–294. (b) Reed, C. A. "Electrochemical and Spectrochemical Studies of Biological Redox Components"; Kadish, K. M., Ed.; Advances in Chemistry 201; American Chemical Society: Washington, DC, 1982; pp 333–356.

(9) Wolberg, A.; Manassen, J. *J. Am. Chem. Soc.* **1970**, *92*, 2982–2991.

(10) (a) Felton, R. H.; Owen, G. S.; Dolphin, D.; Fajer, J. *J. Am. Chem. Soc.* **1971**, *93*, 6332–6334. (b) Felton, R. H.; Owen, G. S.; Dolphin, D.; Forman, A.; Borg, D. C.; Fajer, J. *Ann. N.Y. Acad. Sci.* **1973**, *206*, 504–514.

(11) (a) Phillippi, M. A.; Goff, H. M. *J. Am. Chem. Soc.* **1979**, *101*, 7641–7643. (b) Phillippi, M. A.; Shimomura, E. T.; Goff, H. M. *Inorg. Chem.* **1981**, *20*, 1322–1325. (c) Phillippi, M. A.; Goff, H. M. *J. Am. Chem. Soc.* **1982**, *104*, 6026–6034. (d) Boersma, A. D.; Goff, H. M. *Inorg. Chem.* **1984**, *23*, 1671–1676.

(12) (a) Groves, J. T.; Nemo, T. E.; Myers, R. S. *J. Am. Chem. Soc.* **1979**, *101*, 1032–1033. (b) Groves, J. T.; Kruper, W. J.; Nemo, T. E.; Myers, R. S. *J. Mol. Catal.* **1980**, *7*, 169–177. (c) Groves, J. T.; Haushalter, R. C.; Nakamura, M.; Nemo, T. E.; Evans, B. J. *J. Am. Chem. Soc.* **1981**, *103*, 2884–2886. (d) Groves, J. T.; Quinn, R.; McMurry, T. J.; Nakamura, M.; Lang, G.; Boso, B. *J. Am. Chem. Soc.* **1985**, *107*, 354–360.

(13) Chang, C. K.; Kuo, M. S. *J. Am. Chem. Soc.* **1979**, *101*, 3413–3415.

(14) (a) Chin, D. H.; Del Gaudio, J.; La Mar, G. N.; Balch, A. L. *J. Am. Chem. Soc.* **1977**, *99*, 5486–5488. (b) Chin, D. H.; Balch, A. L.; La Mar, G. N. *J. Am. Chem. Soc.* **1980**, *102*, 1446–1448. (c) Chin, D. N.; La Mar, G. N.; Balch, A. L. *J. Am. Chem. Soc.* **1980**, *102*, 4344–4350. (d) Chin, D. H.; La Mar, G. N.; Balch, A. L. *J. Am. Chem. Soc.* **1980**, *102*, 5945–5947. (e) Balch, A. L.; Chan, Y. W.; Cheng, R. J.; La Mar, G. N.; Latos-Grazynski, L.; Renner, M. W. *J. Am. Chem. Soc.* **1984**, *106*, 7779–7793. (f) Balch, A. L.; Latos-Grazynski, L.; Renner, M. W. *J. Am. Chem. Soc.* **1985**, *107*, 2983–2985.

(15) Simmoneaux, G.; Scholz, W. F.; Reed, C. A.; Lang, G. *Biochim. Biophys. Acta* **1982**, *716*, 1–7.

(16) Abbreviations used in this paper: TPP = *meso*-tetraphenylporphyrinato; Phox = phenoxathiin; TmTP = *meso*-tetra-*m*-tolylporphyrinato; TpTP = *meso*-tetra-*p*-tolylporphyrinato; OEP = octaethylporphinato; Thian = thianthrene.

(17) Gans, P.; Marchon, J. C.; Reed, C. A.; Regnard, J. R. *Nouv. J. Chim.* **1981**, *5*, 203–204.

(18) Buisson, G.; Deronzier, A.; Duée, E.; Gans, P.; Marchon, J. C.; Regnard, J. R. *J. Am. Chem. Soc.* **1982**, *104*, 6793–6796.

(19) Scholz, W. F.; Reed, C. A.; Lee, Y. J.; Scheidt, W. R.; Lang, G. *J. Am. Chem. Soc.* **1982**, *104*, 6791–6793.

(20) Schulz, C. E.; Devaney, P. W.; Winkler, H.; Debrunner, P. G.; Doan, N.; Chiang, R.; Rutter, R.; Hager, L. P. *FEBS Lett.* **1979**, *103*, 102.

(21) Gagne, R. R.; Koval, C. A.; Lisensky, G. C. *Inorg. Chem.* **1980**, *19*, 2854–2855.

(22) Adler, A. D.; Longo, F. R.; Kampas, F.; Kim, J. *J. Inorg. Nucl. Chem.* **1970**, *32*, 2443–2445.

(23) Fleischer, E. B.; Srivastava, T. S. *J. Am. Chem. Soc.* **1969**, *91*, 2403–2405.

phenoxathiin (Kodak), antimony pentachloride (Merck), and ferric perchlorate nonahydrate (Fluka) were used as received.

Syntheses. Because the oxidized iron porphyrin complexes reported in this paper are decomposed easily to iron(III) porphyrin species, oxidation resistant solvents such as dichloromethane, 1,1,2,2-tetrachloroethane, and hexane were used. Care was taken to exclude trace water, but scrupulously inert atmosphere techniques were not usually necessary.

(Phox^{+}·)SbCl$_6$. The radical cation of phenoxathiin was obtained in microcrystalline, analytically pure form as the hexachloroantimonate salt by the following method. To a solution of phenoxathiin (10 g) in dichloromethane (300 mL) was added a solution of antimony pentachloride (12 g) in dichloromethane (100 mL). Phenoxathiinylium hexachloroantimonate precipitated immediately as a violet microcrystalline powder which was quickly filtered under a stream of argon, dried under vacuum, and stored in a dry atmosphere. Anal. Calcd for $C_{12}H_8Cl_6SSb$: C, 26.95; H, 1.51; Cl, 39.78. Found: C, 26.58; H, 1.63; Cl, 39.18. IR (KBr): 1595, 1550, 1465, 1350, 1280, 1080, 895, 760 cm^{-1}. Magnetic moment (300 K, uncor): μ_{eff} = 1.6 μ_B. The shelf life of this material is <6 weeks in a drybox.

(Thian^{+}·)ClO$_4$. The thianthrene radical cation perchlorate was prepared by a modification of the synthesis of Shine et al.[25] Thianthrene (0.5 g) was dissolved in dichloromethane (20 mL), and perchloric acid (1 mL) was added. The colorless solution was stireed for 10 min, and the acid layer gradually became dark blue. Acetic anhydride (ca. 5 mL) was slowly added under nitrogen, causing the entire solution to turn dark blue. The solution was refrigerated for 12 h and then filtered under nitrogen to recover blue-bronze crystals which were washed with dry toluene and dried in vacuo (0.30 g, 40%). **Caution**: This perchlorate salt is prone to detonation after long storage and should be used soon after preparation. The product crystallized with half a molecule of dichloromethane. Anal. Calcd for $C_{12.5}H_9S_2O_4Cl_2$: C, 41.91; H, 2.53; S, 17.90. Found: C, 41.80; H, 2.72; S, 18.5. IR (KBr): 1590, 1475, 1315, 1080, 1010, 822, 620 cm^{-1}.

[FeCl(TPP·)][SbCl$_6$] (1). FeCl(TPP) (0.5 g, 0.71 mmole) was dissolved in dichloromethane (25 mL) and the solution was stirred for 30 min. (Phox^{+}·SbCl$_6^{-}$ (0.4 g, 0.75 mmol) was then added, and the suspension was stirred for 45 min. After filtration, hexane (20 mL) was slowly added to the filtrate. Fine black needles of the product were obtained by filtration after overnight crystallization; they were washed with 20 mL of a 1:1 dichloromethane–hexane mixture, then with 10 mL of hexane, and dried by aspiration (0.67 g, 89%). Analysis is consistent with a dichloromethane solvate of composition [FeCl(TPP·)][SbCl$_6$]·$^1/_4$CH$_2$Cl$_2$. Anal. Calcd for $C_{177}H_{114}Cl_{30}Fe_4N_{16}Sb_4$: C, 50.15; H, 2.71; Cl, 25.09; Fe, 5.27; N, 5.29. Found: C, 49.80; H, 2.62; Cl, 23.50; Fe, 5.33; N, 5.12. IR (KBr): 1340, 1280, 1000, 800, 750, 725, 700 cm^{-1}. Analogous meta- or para-substituted tetratolylporphyrin complexes were prepared and isolated in the same manner. Attempts to isolate the ortho-substituted analogue were unsuccessful.

Crystals of [FeCl(TPP·)][SbCl$_6$] for X-ray Crystallography. [FeCl(TPP·)][SbCl$_6$]·$^1/_4$CH$_2$Cl$_2$ (1 g) was dissolved in 20 mL of 1,1,2,2-tetrachloroethane. A layer of 5 mL of hexane was carefully added over the top of the solution. Slow diffusion of hexane afforded large needle-shaped single crystals of a 1,1,2,2-tetrachloroethane solvate of composition [FeCl(TPP·)][SbCl$_6$]·$^1/_2$CH$_2$Cl$_4$ which were collected by filtration after one week (0.45 g, 42%). Anal. Calcd for $C_{45}H_{29}Cl_9FeN_4Sb$: C, 48.15; H, 2.60; Cl, 28.43; Fe, 4.98; N, 4.99; Sb, 10.85. Found: C, 48,30; H, 2.65; Cl, 25.72; Fe, 5.05; N, 4.93; Sb, 11.54. Single crystals of a 1,1,2,2-tetrachloroethane solvate of the analogous para-substituted tetratolylporphyrin (**3**) complex suitable for X-ray diffraction studies were obtained in the same manner.

[FeCl(OEP·)][SbCl$_6$]. FeCl(OEP) (0.075 g, 0.12 mmol) and (Phox^{+}·)SbCl$_6^{-}$ (0.065 g, 0.12 mmol) were stirred in dichloromethane (20 mL) overnight, and the resulting brown precipitate was recovered by filtration, washed with dichloromethane, and dried in vacuo (0.095 g, 83%). Anal. Calcd for $C_{36}H_{44}N_4Cl_7FeSb$: C, 45.11; H, 4.63; N, 5.85; Cl, 25.89. Found: C, 45.14; H, 4.69; N, 5.86; Cl, 25.55. IR (KBr): 2970, 1535, 1440, 1230, 1050 cm^{-1}. λ_{max} (CH_2Cl_2): 355, 520, 579 nm.

Fe(OClO$_3$)$_2$(TPP·) (2). Method A. (FeTPP)$_2$O (0.1 g) and Fe(ClO$_4$)$_3$·9H$_2$O (0.2 g) were stirred in dichloromethane (20 mL). The initial greenish solution turned orange and then dark brown. After 2 h the solution was filtered to remove inorganic solids, and the solution volume was reduced to 10 mL. Heptane (ca. 10 mL) was then slowly added while swirling under nitrogen, and the solution was left in a refrigerator to crystallize overnight. Small purple needles were recovered upon filtration (0.067 g, 45%). **Caution**: Organic perchlorate salts may detonate upon scraping or combustion. The product crystallized with one-quarter of a dichloromethane molecule of solvation. Anal. Calcd for $C_{44.25}H_{28.5}N_4O_4Cl_{2.5}Fe$: C, 59.80; H, 3.23; N, 6.30; Cl, 9.97. Found: C, 60.61; H, 3.05; N, 6.33; Cl, 10.01. IR (KBr): 1330, 1270, 1080, 1000, 800, 750, 720, 700 cm^{-1}.

Method B. Fe(OClO$_3$)(TPP) (0.200 g, 0.26 mmol) and (Thian^{+}·)ClO$_4^{-}$ (0.093 g, 0.29 mmol) were stirred in dichloromethane (25 mL). An orange-brown solution resulted immediately and became dark brown after stirring 1 h. After 2 h the solution was filtered, and the volume was reduced to 10 mL. Heptane (ca. 15 mL) was then slowly added while swirling under nitrogen, and the solution was left in a refrigerator to crystallize overnight. A microcrystalline purple precipitate was recovered upon filtration (0.095 g, 41%). **Caution**: Organic perchlorate salts may detonate upon scraping or combustion. The product crystallized with approximately one-quarter of a dichloromethane molecule of solvation. Anal. Calcd for $C_{44.25}H_{28.5}N_4O_4Cl_{2.5}Fe$: C, 59.80; H, 3.23; N, 6.30; Cl, 9.97. Found: C, 59.72; H, 3.13; N, 6.21; Cl, 9.76. This solvation is not apparent in the single-crystal X-ray structure, but repeatedly consistent analyses require its presence in bulk samples. Analogous ortho-, meta-, or para-substituted tetratolylporphyrin complexes were obtained in a similar manner.

Single crystals of Fe(OClO$_3$)$_2$(TPP·) marginally suitable for X-ray diffraction studies were grown by slow diffusion of heptane into a concentrated solution of the complex in dichloromethane.

X-ray Structure Determination. Crystals of **3** used for data collection were glued on glass fibers in air, mounted on an Enraf-Nonius CAD4 automatic diffractometer, centered in the beam, and cooled to −140 °C. After automatic searches of reciprocal space and indexing of the discovered reflections, the reflections were examined for intensity and peak width. Reflections with higher sin θ/λ values were then located, and the cell dimensions were refined against their setting angles. The final crystal parameters are given in Table I together with details of the data collection procedure.

Of the 7876 data collected, 4627 had $F_o > 2\sigma(F_o)$ and were used for the structure solution and refinement. The structure was solved by standard heavy-atom techniques. The Sb and Fe atoms were located by Patterson synthesis, and they were used to obtain an initial electron-density map. This readily gave the positions of the six chlorine atoms of the SbCl$_6$ anion, the chlorine axial ligand, the nitrogen and carbon atoms of the porphyrin, and one tetrachloroethane solvate molecule (named S). At this stage, several remaining peaks as intense as those of chlorine atoms could not be interpreted. They were eventually assigned to two sites for disordered solvate molecules (named T and U). The latter share a common site for the chlorine atom TUCCl. It was found that sites T and U are exclusive of each other, with an occupancy ratio of 0.55/0.45. It was not possible to locate the carbon atoms of T and U by difference Fourier methods. Thus, their best positioned parameters were calculated from the coordinates of the corresponding chlorine atoms. Therefore, no thermal parameters for these atoms appear in Table A. The final values of the discrepancy indexes were R = 0.088 and R_w = 0.097. Final atomic coordinates are listed in Table II.

The structure of the bis(perchlorato) complex **2** was solved in a straightforward manner by using the same general procedure. Crystal data, as well as details on the collection of diffracted intensities, are given in Table I. The final values of the discrepancy indexes were R = 0.116 and R_w = 0.130. Final atomic coordinates are listed in Table III.

Table I. Crystal and Data Collection Parameters for [FeCl(TpTP·)]SbCl$_6$·2C$_2$H$_2$Cl$_4$ and Fe(OClO$_3$)$_2$(TPP·)

	[FeCl(TpTP·)]-SbCl$_6$·2C$_2$H$_2$cl$_4$[a]	Fe(OClO$_3$)$_2$(TPP·)[b]
formula	(C$_{48}$H$_{36}$N$_4$ClFe)-(SbCl$_6$)·2C$_2$H$_2$-Cl$_4$	(C$_{44}$H$_{28}$N$_4$Cl$_2$FeO$_8$)
M_r	1430.3	867.5
space group	$P2_1/c$	$P2_1/c$
a, Å	10.98 (1)	12.132 (1)
b, Å	22.57 (1)	14.662 (1)
c, Å	23.65 (1)	13.153 (1)
β, deg	97.73 (5)	127.84 (1)
V, Å^3	5808	1842
Z	4	2
radiation	Mo Kα (graphite monochromator)	Cu Kα (Ni filtered)
2θ range, deg	1–44	1–156
scan type	θ–2θ	θ–2θ
no. of reflcns collected	7876	4001
unique reflcns used in least-squares fit	4627 with $F_o > 2\sigma(F_o)$	1448 with $F_o > 3\sigma(F_o)$

[a] Crystal parameters at −140 °C. [b] Crystal parameters at 25 °C.

(24) Reed, C. A.; Mashiko, T.; Bentley, S. P.; Kastner, M. E.; Scheidt, W. R.; Spartalian, K.; Lang, G. *J. Am. Chem. Soc.* **1979**, *101*, 2948–2958.
(25) Murata, Y.; Shine, H. J. *J. Org. Chem.* **1969**, *34*, 3368–3372.

Table II. Atomic Coordinates in the Unit Cell of $[FeCl(TpTP\cdot)][SbCl_6]\cdot 2C_2H_2Cl_4$

atom	10^4x	10^4y	10^4z	atom	10^4x	10^4y	10^4z	atom	10^4x	10^4y	10^4z
Sb	2156 (1)	8096 (1)	2579 (1)	C14	-3914 (14)	5036 (7)	-1222 (6)	C40	-706 (15)	2504 (7)	654 (7)
Cl1	2266 (5)	8673 (3)	3407 (2)	C15	-4129 (14)	4440 (7)	-1313 (6)	C41	-364 (16)	1903 (8)	698 (7)
Cl2	2165 (7)	7528 (3)	1748 (2)	C16	-3559 (15)	3983 (7)	-971 (6)	C42	-90 (16)	1585 (7)	218 (8)
Cl3	943 (6)	8802 (3)	2039 (2)	C17	-3855 (15)	3372 (7)	-1001 (7)	C43	-132 (15)	1878 (8)	-306 (7)
C14	3929 (6)	8578 (4)	2356 (2)	C18	-3000 (14)	3076 (8)	-616 (6)	C44	-466 (14)	2471 (8)	-361 (7)
Cl5	454 (7)	7582 (5)	2805 (3)	C19	-2197 (15)	3526 (7)	-355 (6)	C45	2093 (18)	5777 (9)	3394 (7)
Cl6	3391 (8)	7379 (3)	3092 (2)	C20	-1178 (14)	3413 (7)	54 (6)	C46	-4090 (18)	8688 (7)	-683 (8)
Fe	-2435 (2)	4813 (1)	-35 (1)	C21	352 (13)	5381 (7)	1688 (6)	C47	-7959 (19)	37557 (11)	-3158 (8)
Cl	-3838 (4)	4601 (2)	496 (2)	C22	1019 (14)	5903 (7)	1786 (7)	C48	257 (18)	932 (7)	261 (9)
N1	-906 (11)	4422 (5)	439 (5)	C23	1585 (14)	6034 (8)	2333 (7)	SCl1	5253 (6)	18 (2)	8253 (2)
N2	-1769 (11)	5622 (6)	294 (5)	C24	1485 (14)	5632 (8)	2785 (7)	SCl2	6633 (8)	1363 (3)	9438 (3)
N3	-3324 (10)	5276 (6)	-717 (5)	C25	776 (15)	5127 (8)	2684 (7)	SCl3	4495 (9)	339 (3)	9328 (3)
N4	-2558 (11)	4083 (6)	-555 (5)	C26	224 (14)	4995 (7)	2127 (6)	SCl4	7409 (10)	150 (4)	9346 (5)
C1	-556 (14)	3847 (7)	408 (6)	C27	-3579 (15)	6892 (8)	-397 (6)	SC1	5299 (22)	586 (9)	8779 (8)
C2	498 (14)	3735 (8)	824 (6)	C28	-2787 (15)	7374 (7)	-363 (7)	SC2	6595 (22)	747 (10)	8985 (10)
C3	728 (13)	4248 (7)	1127 (6)	C29	-3218 (15)	7950 (8)	-449 (6)	TUCl1	7204 (6)	6136 (3)	7278 (3)
C4	-173 (13)	4676 (7)	891 (6)	C30	-4495 (19)	8065 (8)	-566 (7)	TCl2	7391 (8)	7161 (4)	8029 (3)
C5	-335 (13)	5240 (7)	1110 (6)	C31	-5315 (16)	7582 (8)	-571 (7)	TCl3	5800 (16)	7256 (6)	6797 (7)
C6	-1132 (13)	5668 (7)	837 (6)	C32	-4875 (15)	7013 (7)	-504 (6)	TCl4	7666 (17)	6908 (7)	6283 (5)
C7	-1367 (15)	6229 (7)	1076 (7)	C33	-5101 (15)	4257 (7)	-1791 (7)	TC1	7770 (0)	6860 (0)	7390 (0)
C8	-2161 (15)	6530 (7)	673 (7)	C34	-6253 (16)	4546 (8)	-1844 (7)	TC2	7930 (0)	7260 (0)	6920 (0)
C9	-2407 (13)	6143 (7)	185 (7)	C35	-7174 (16)	4383 (9)	-2285 (7)	UCl2	8024 (14)	5977 (6)	6112 (6)
C10	-3118 (14)	6277 (7)	-323 (6)	C36	-6935 (17)	3937 (8)	-2677 (7)	UCl3	7392 (9)	7662 (7)	6932 (4)
C11	-3469 (15)	5880 (7)	-764 (6)	C37	-5787 (17)	3650 (9)	-2632 (7)	UCl4	5983 (12)	6967 (6)	6001 (5)
C12	-4083 (15)	6033 (8)	-1327 (6)	C38	-4846 (16)	3825 (8)	-2182 (7)	UC1	7820 (0)	6450 (0)	6700 (0)
C13	-4352 (15)	5511 (7)	-1607 (7)	C39	-768 (15)	2786 (7)	124 (6)	UC2	7280 (0)	7020 (0)	6500 (0)

Table III. Atomic Coordinates in the Unit Cell of $Fe(OClO_3)_2(TPP\cdot)$

atom	10^3x	10^3y	10^3z
Fe	0	0	0
Cl	-239 (1)	32 (1)	-309 (1)
O1	-160 (1)	64 (1)	-172 (1)
O2	-335 (2)	100 (1)	-390 (1)
O3	-134 (2)	16 (2)	-323 (2)
O4	-317 (2)	-47 (1)	-328 (2)
N1	20 (1)	118 (1)	92 (1)
N2	-141 (1)	-48 (1)	23 (1)
C1	106 (2)	188 (1)	119 (2)
C2	95 (2)	262 (1)	190 (2)
C3	-2 (2)	229 (1)	205 (2)
C4	-47 (2)	144 (1)	143 (2)
C5	-140 (2)	85 (1)	142 (2)
C6	-193 (2)	-3 (1)	81 (2)
C7	-306 (2)	-50 (1)	62 (2)
C8	-329 (2)	-129 (1)	-9 (2)
C9	-221 (2)	-124 (1)	-29 (2)
C10	-209 (2)	-192 (1)	-99 (2)
C11	-185 (2)	115 (1)	223 (2)
C12	-256 (3)	193 (2)	199 (2)
C13	-302 (3)	218 (2)	273 (2)
C14	-266 (3)	160 (2)	374 (2)
C15	-187 (3)	81 (2)	402 (2)
C16	-145 (2)	52 (1)	326 (2)
C17	-308 (2)	-268 (1)	-154 (2)
C18	-310 (2)	-336 (1)	-76 (2)
C19	-403 (2)	-407 (2)	-131 (2)
C20	-501 (2)	-416 (2)	-265 (2)
C21	-500 (2)	-348 (2)	-343 (2)
C22	-407 (2)	-276 (2)	-288 (2)

Magnetic Susceptibility. Data were collected on ~25-mg finely ground samples in aluminum or Kel-F buckets by using an SHE Model 905 SQUID Susceptometer or on 100–250-mg samples by using a Faraday balance at the CNRS Louis Néel Laboratory. Comparison of data at 2 kG and 10 kG were the same within 1%, indicating that crystal alignment within the magnet field was not occurring. All data were corrected for diamagnetism (χ_{dia}) by using the literature value for H_2TPP[26] and Pascal's constants for the remaining atoms or groups.[27] Values of -872×10^{-6} and -791×10^{-6} cgs units were applied to **1** and **2**, respectively.

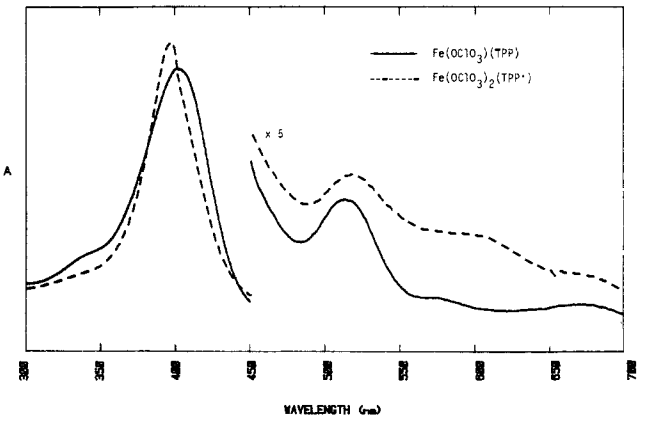

Figure 1. UV-vis spectra of $Fe(OClO_3)(TPP)$ (solid line) and $Fe(OClO_3)_2(TPP\cdot)$ (dashed line) at same concentration in dichloromethane.

Data were fit to the simple $-2J$ spin Hamiltonian $\mathcal{H} = -2J\mathbf{S}_1\cdot\mathbf{S}_2$ for an $S = {}^5/_2$, $S = {}^1/_2$ system[28] by visual comparison of the data to computer-derived theoretical curves. Values of the gyromagnetic ratio, g, were obtained from the slope of the linear portion of the Curie plot by using a rearranged form of the equation

$$\chi_M = \frac{Ng^2\beta^2S(S+1)}{3kT}$$

Values of the Weiss constant, θ, were obtained by extrapolation of a least-squares fit to the linear portion of the Curie plot.

Results

Electronic Spectra. The electronic absorption spectrum of $[FeCl(TPP\cdot)][SbCl_6]$ has been reported previously[8b] and is essentially identical with $[FeCl(TPP\cdot)]^+$ produced electrochemically.[9-11] It shows the characteristics of a porphyrin cation radical,[29] including a broad α,β region, new absorption bands above 700 nm, and a Soret band (388 nm) that is broadened, blue-shifted, and lowered in intensity compared to FeCl(TPP). These characteristics are also present in the spectrum of $Fe(OClO_3)_2(TPP\cdot)$, although in this case the Soret band (396 nm) has "normal" intensity (Figure 1). The shape of these spectra is unusually sensitive to the presence of a methyl substituent at the ortho, meta, or para position of the phenyl rings, as illustrated

(26) Eaton, S. S.; Eaton, G. R. *Inorg. Chem.* **1980**, *19*, 1095–1096.
(27) Boudreaux, E. A.; Mulay, L. N. "Theory and Applications of Molecular Paramagnetism"; Wiley: New York, 1976; p 491 ff.
(28) Wojciechowski, W. *Inorg. Chim. Acta* **1967**, *1*, 319.
(29) Fuhrhop, J. H. *Struct. Bonding (Berlin)* **1974**, *18*, 1–67.

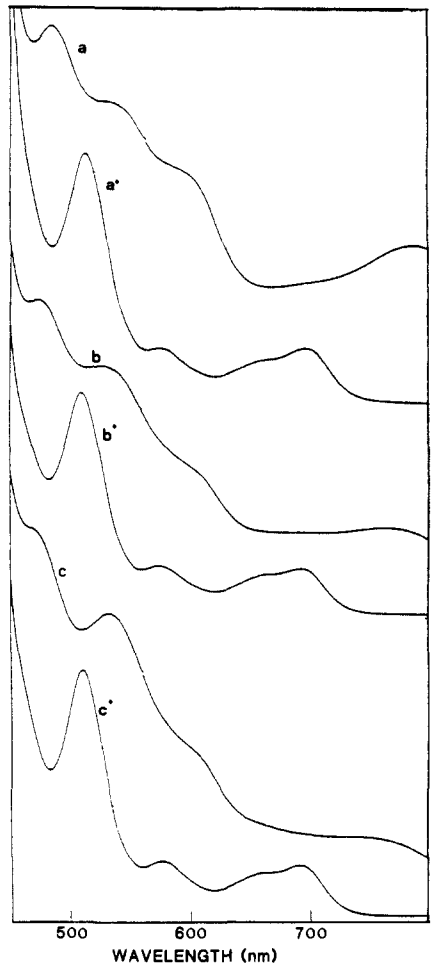

Figure 2. Vis spectra of oxidized and parent tolyl derivatives in dichloromethane: (a) $[FeCl(TpTP\cdot)]^+$, (a') FeCl(TpTP), (b) $[FeCl(TmTP\cdot)]^+$, (b') FeCl(TmTP), (c) $[FeCl(TPP\cdot)]^+$, (c') FeCl(TPP).

in Figure 2 for the chloro species. A similar effect is observed with the perchlorato species, This probably reflects different delocalization patterns of the charge density on the porphyrin macrocycle due to inductive effects of the phenyl substituents.

Infrared Spectra. In addition to exhibiting absorptions normally found in iron tetraphenylporphyrin complexes, both oxidized complexes show a new band near 1280 cm^{-1} which we believe to be a diagnostic tetraphenylporphyrin π-cation radical absorption,[30] $[FeCl(TPP\cdot)][SbCl_6]$ also shows absorptions at 375 (Fe–Cl stretch) and 340 cm^{-1} (Sb–Cl stretch). The spectrum of $Fe(OClO_3)_2(TPP\cdot)$ exhibits several new bands at 610, 620, 630, 640, 870, 1125, 1150, 1160, and 1170 cm^{-1} which can be assigned to Cl–O stretching modes of coordinated perchlorate.[24,31] All the infrared characteristics described above are also found in the various tetratolylporphyrin complexes,

In the octaethylporphyrin complex $[FeCl(OEP\cdot)][SbCl_6]$ we find a strong new absorption at 1535 cm^{-1} relative to FeCl(OEP) that appears to be diagnostic of the OEP radical cation. This is illustrated in Figure 3.

Electrochemistry. The electrochemical behavior of the $FeCl(TPP)/[FeCl(TPP)]^+$ couple has been described several times,[9-11] and it will not be reported again here. On the other hand, we have shown recently that electrochemical oxidation of $[Fe(H_2O)_2(TPP)][ClO_4]$ in dichloromethane at a potential corresponding to the first oxidation wave ($E_{1/2}$ = 1.12 V vs. SCE) is a one-electron reversible process.[32] Exhaustive electrolysis at

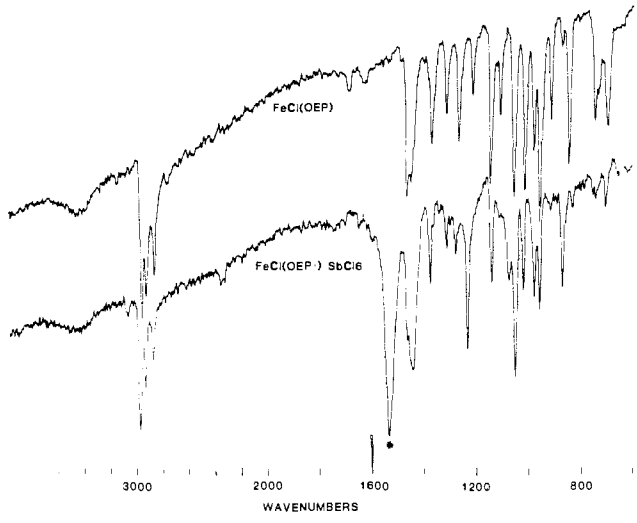

Figure 3. Comparison of infrared spectra (KBr) of FeCl(OEP) and $[FeCl(OEP)][SbCl_6]$. The diagnostic OEP radical cation band (*) is seen at 1535 cm^{-1}.

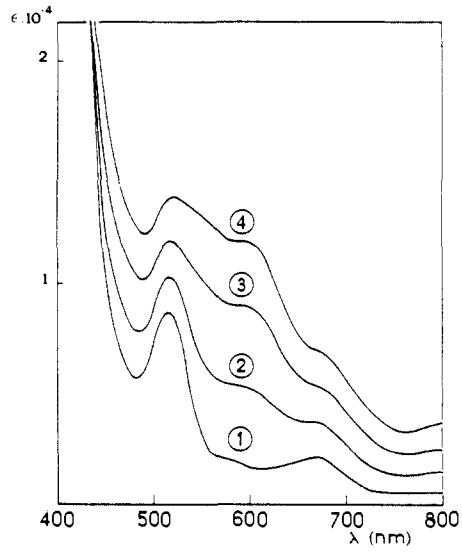

Figure 4. Vis spectra recorded during the electrolysis of $[Fe(H_2O)_2(TPP)][ClO_4]$ in dichloromethane in the presence of 10^{-1} M $[Bu_4N][ClO_4]$: 1, $[Fe(H_2O)_2(TPP)][ClO_4]$; 2, after 33% electrolysis; 3, after 66% electrolysis; 4, $Fe(OClO_3)_2(TPP\cdot)$.

Table IV. Chemical Shift Values (ppm) for the Protons in $[FeCl(TPP\cdot)][SbCl_6]$ and $Fe(OClO_3)_2(TPP\cdot)$ and Their *m*- and *p*-Tolyl Derivatives[a]

compound	pyrrole	ortho	meta	para	methyl
$[FeCl(TPP\cdot)][SbCl_6]$	68.8	42.2	-12.3	35.0	
$[FeCl(TpTP\cdot)][SbCl_6]$	64.8	48.0	-14.7		-30.5
$[FeCl(TmTP\cdot)][SbCl_6]$	68.7	44.5, 42.6	-13.0	37	5.94
$Fe(OClO_3)_2(TPP\cdot)$	31.1	-19.3	35.0	-13.2	
$Fe(OClO_3)_2(TpTP\cdot)$	31.6	-16.9	31.6		0.10
$Fe(OClO_3)_2(TmTP\cdot)$	28.2	-16.0, -17.9	30.8	-11.3	-0.50

[a] 25 °C, dichloromethane.

1.3 V requires 1.0 ± 0.1 faraday/mol and affords a solution whose electronic spectrum is identical with that of $Fe(OClO_3)_2(TPP\cdot)$. Spectral changes during electrolysis are shown in Figure 4. The electrochemical behavior of $Fe(OClO_3)_2(TPP\cdot)$ parallels that of the final oxidized solution described above. Half-wave potentials have the same values within experimental error in both cases. Moreover, reductive electrolysis at +0.6 V of a $Fe(OClO_3)_2(TPP\cdot)$ solution requires 1.0 ± 0.1 faraday/mol, and it yields a species which has a visible spectrum identical with that of $[Fe(H_2O)_2(TPP)][ClO_4]$.

NMR Spectra. As also noted by Goff,[11] oxidized iron porphyrin complexes yield well-resolved proton NMR spectra which differ

(30) Shimomura, E. T.; Phillippi, M. A.; Goff, H. M.; Scholz, W. F.; Reed, C. A. *J. Am. Chem. Soc.* **1981**, *103*, 6778–6780.
(31) Nakamoto, K. "Infrared and Raman Spectra of Inorganic and Coordination Compounds", 3rd ed.; Wiley: New York, 1977; p 242.
(32) Arena, F.; Gans, P.; Marchon, J. C. *J. Chem. Soc., Chem. Comm.* **1984**, 196–197. Arena, F.; Gans, P.; Marchon, J. C. *Nouv. J. Chim.*, in press.

Table V. Mössbauer Parameters Relative to Iron Metal at Room Temperature

compound	temp, K	$\delta \pm 0.02$, mm s^{-1}	$\Delta E_Q \pm 0.02$, mm s^{-1}	$\Gamma_1 \pm 0.02$, mm s^{-1}	$\Gamma_2 \pm 0.02$, mm s^{-1}
[FeCl(TPP·)][$SbCl_6$]	1.8	0.41	0.50	0.40	0.41
	4.2	0.41	0.56	0.47	0.43
	20	0.41	0.56	0.32	0.32
	77	0.40	0.55	0.32	0.35
	300	0.28	0.52	0.42	0.44
FeCl(TPP)	4.2	0.43	0.46		
$Fe(OClO_3)_2$(TPP·)	2	0.48	1.77	0.49	0.49
	4.2	0.48	1.78	0.54	0.54
	77	0.46	1.76	0.41	0.51
	300	0.35	1.86	0.32	0.46
[$Fe(Me_2SO)_2$(TPP)][ClO_4]	4.2	0.45	1.22	*a*	*a*
[$Fe(C_2H_5OH)_2$(TPP)][BF_4]	4.2	0.42	1.89	*b*	*b*
[$Fe(H_2O)_2$(TPP)][ClO_4]	78	0.41	1.53	*c*	*c*

[a] Reference 38. [b] Reference 37. [c] Reference 36.

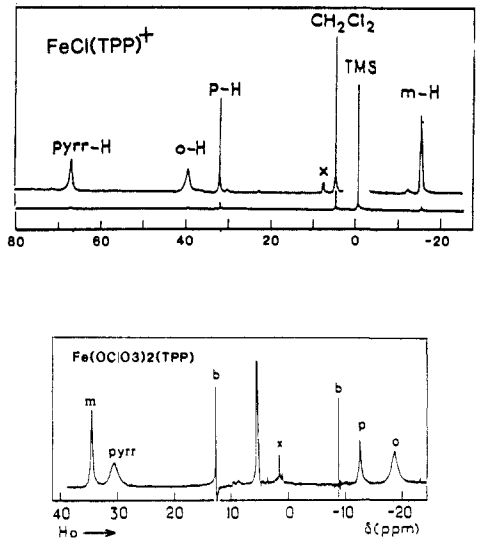

Figure 5. ^{1}H NMR spectra of [FeCl(TPP·)][$SbCl_6$] (upper) and Fe($OClO_3$)$_2$(TPP·) (lower) in dichloromethane-d_2 at 25 °C. Peaks labeled × are impurities; those labeled b are instrument glitches. Peaks were assigned to pyrrole, ortho, meta, and para hydrogens by comparison to the coresponding tolyl derivatives.

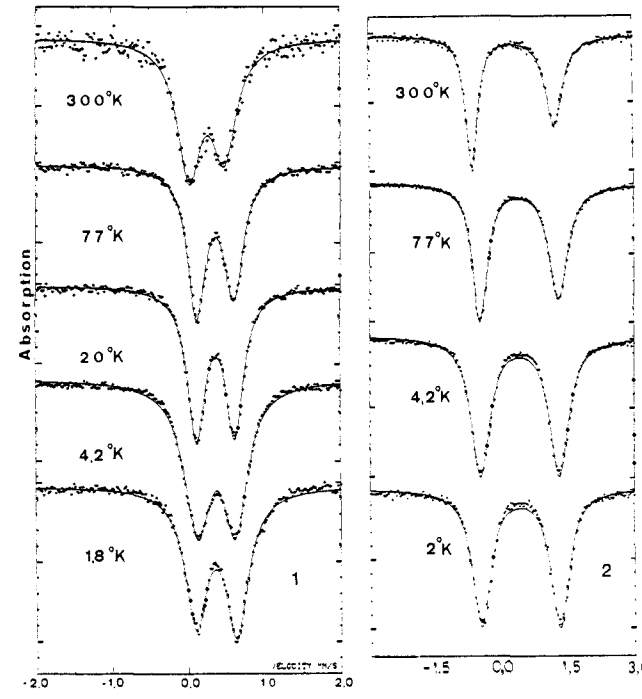

Figure 6. Mössbauer spectra of [FeCl(TPP·)][$SbCl_6$] (**1**) (left) and Fe($OClO_3$)$_2$(TPP·) (**2**) (right) as a function of temperature.

from parent iron(III) spectra most significantly by the magnitude of phenyl proton isotropic shifts. Proton NMR spectra of [FeCl(TPP·)][$SbCl_6$] and Fe($OClO_3$)$_2$(TPP·) at room temperature are shown in Figure 5. Resonances for the meta and para tetratolylporphyrin derivatives are listed in Table IV. Cross comparison leads to assignment of resonances for all species.

Splitting of the ortho and meta phenyl proton resonances of [FeCl(TPP·)][$SbCl_6$] is observed as the temperature is lowered below −5 °C (ortho) or −15 °C (meta). This indicates unsymmetrical axial ligation in the complex,[33] a feature which is apparent from its formula, but the question of hexachloroantimonate binding to iron cannot be resolved by this observation. The structure of the complex in the solid state shows an uncoordinated hexachloroantimonate anion (vide infra), and this is assumed to persist in solution.

The temperature variations of the proton resonances of [FeCl(TPP·)][$SbCl_6$] are summarized in Figure A of the supplementary material. Plots of δ vs. $1/T$ are linear within the range 35 to −90 °C for pyrrole protons and within the range −10 to −90 °C for phenyl protons. Appreciable curvature of the Curie plots for the phenyl protons above −10 °C can be correlated to the observation that ortho and meta phenyl resonances coalesce at about the same temperature.

A study of the temperature variation of the proton resonances of Fe($OClO_3$)$_2$(TPP·) could not be done due to precipitation of the complex as the temperature is lowered below 0 °C.

Mössbauer Spectroscopy. Mössbauer spectra of crystalline samples of **1** and **2** at various temperatures between 300 and 1.8 K are shown in Figure 6. Table V summarizes the parameters derived from these experiments. The Mössbauer spectrum of [FeCl(TPP·)][$SbCl_6$] (**1**) shows two broad, asymmetric absorption lines whose relative intensities vary with temperature. The isomer shift and quadrupole splitting values are in the range of those observed for five-coordinate high-spin iron(III) porphyrins (δ = 0.25–0.40 mm/s; ΔE_Q = 0.4–1.0 mm/s),[34] and the temperature independence of ΔE_Q is consistent with a high-spin Fe(III) state.[35] The Mössbauer parameters of Fe($OClO_3$)$_2$(TPP·) are typical of six-coordinate high-spin iron(III) porphyrins (δ = 0.32–0.45 mm/s; ΔE_Q = 1.22–2.07 mm/s); the larger values of the quadrupole splitting in six-coordinate high-spin compounds, compared to those found in five-coordinate compounds, have already been noted and discussed.[36-38]

(33) La Mar, G. N.; Walker, F. A. "The Porphyrins"; Dolphin, D., Ed.; Academic Press: New York, 1978; Vol. 4, pp 61–157.

(34) Sams, J. R.; Tsin, T. B. "The Porphyrins"; Dolphin, D., Ed.; Academic Press: New York, 1978; Vol. 4, pp 425–478.

(35) Greenwood, N. N.; Gibb, T. C. "Mossbauer Spectroscopy"; Chapman and Hall: London, 1971; Chapter 5.

(36) Scheidt, W. R.; Cohen, I. A.; Kastner, M. E. *Biochemistry* **1979**, *18*, 3546–3552.

(37) Gans, P.; Buisson, G.; Duee, E.; Regnard, J. R.; Marchon, J. C. *J. Chem. Soc., Chem. Commun* **1978**, 393–395.

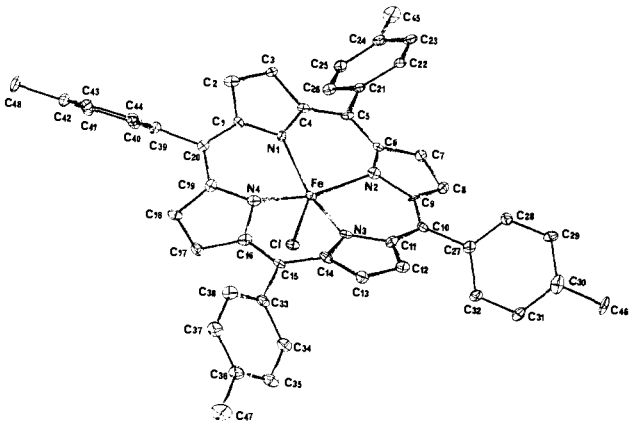

Figure 7. An ORTEP drawing of the five-coordinate cation $[FeCl(TpTP\cdot)]^+$ showing the atom numbering scheme. Thermal ellipsoids are contoured at the 50% probability level (−140 °C).

Table VI. Bond Distances (Å) with Standard Deviations in $[FeCl(TpTP\cdot)][SbCl_6]\cdot 2C_2H_2Cl_4$

Fe-N1	2.09 (1)	C27-C28	1.39 (2)
Fe-N2	2.08 (1)	C28-C29	1.39 (2)
Fe-N3	2.05 (1)	C29-C30	1.42 (3)
Fe-N4	2.05 (1)	C30-C31	1.42 (3)
Fe-Cl	2.168 (5)	C31-C32	1.38 (2)
N1-C1	1.36 (2)	C32-C27	1.44 (2)
N1-C4	1.37 (2)	C30-C46	1.52 (3)
N2-C6	1.38 (2)		
N2-C9	1.38 (2)	C33-C34	1.41 (2)
N3-C11	1.37 (2)	C34-C35	1.40 (2)
N3-C14	1.39 (2)	C35-C36	1.42 (3)
N4-C16	1.39 (2)	C36-C37	1.41 (3)
N4-C19	1.38 (2)	C37-C38	1.44 (2)
C1-C2	1.44 (2)	C38-C33	1.40 (2)
C2-C3	1.37 (2)	C36-C47	1.54 (3)
C3-C4	1.44 (2)		
C4-C5	1.39 (2)	C39-C40	1.40 (2)
C5-C6	1.40 (2)	C40-C41	1.41 (2)
C6-C7	1.42 (2)	C41-C42	1.41 (3)
C7-C8	1.38 (2)	C42-C43	1.40 (3)
C8-C9	1.44 (2)	C43-C44	1.39 (2)
C9-C10	1.38 (2)	C44-C39	1.43 (2)
C10-C11	1.39 (2)	C42-C48	1.52 (2)
C11-C12	1.45 (2)		
C12-C13	1.36 (2)	Sb-Cl1	2.340 (5)
C13-C14	1.45 (2)	Sb-Cl2	2.350 (6)
C14-C15	1.38 (2)	Sb-Cl3	2.343 (6)
C15-C16	1.41 (2)	Sb-Cl4	2.351 (7)
C16-C17	1.42 (2)	Sb-Cl5	2.322 (9)
C17-C18	1.39 (2)	Sb-Cl6	2.342 (7)
C18-C19	1.43 (2)		
C19-C20	1.40 (2)	SCl1-SC1	1.78 (2)
C20-C1	1.41 (2)	SCl-SCl3	1.76 (2)
		SC1-SC2	1.49 (3)
C5-C21	1.51 (2)	SC2-SCl2	1.75 (2)
C10-C27	1.48 (2)	SC2-SCl4	1.77 (2)
C15-C33	1.50 (2)		
C20-C39	1.49 (2)	TUCl1-TCl	1.755 (7)
		TC1-TCl2	1.757 (8)
		TC1-TC2	1.449 (0)
C21-C22	1.39 (2)	TC2-TCl3	1.73 (1)
C22-C23	1.39 (2)	TC2-TCl4	1.77 (1)
C23-C24	1.42 (2)		
C24-C25	1.38 (2)	TUCl1-UC1	1.755 (7)
C25-C26	1.41 (2)	UC1-UCl2	1.79 (2)
C26-C21	1.38 (2)	UC1-UC2	1.468 (0)
C24-C45	1.54 (2)	UC2-UCl3	1.77 (1)
		UC2-UCl4	1.73 (1)

Description of the Structures. The crystal lattice of $[FeCl(TpTP\cdot)][SbCl_6]$ consists of discrete $[FeCl(TpTP\cdot)]^+$ cations and $[SbCl_6]^-$ anions, and tetrachloroethane molecules occupy the holes resulting from the packing of the porphyrin complex and its

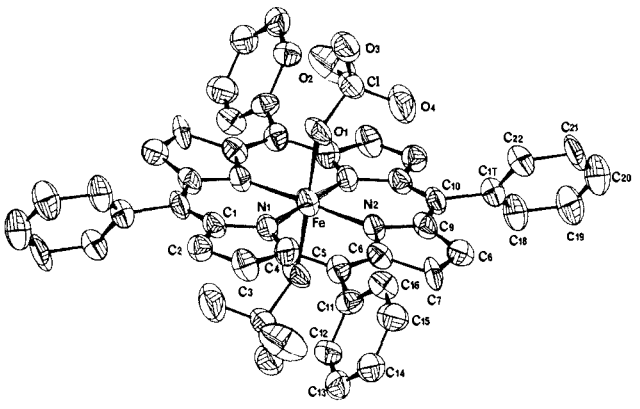

Figure 8. An ORTEP drawing of $Fe(OClO_3)_2(TPP\cdot)$ showing the atom numbering scheme. Thermal ellipsoids are shown at the 50% probability level (20 °C).

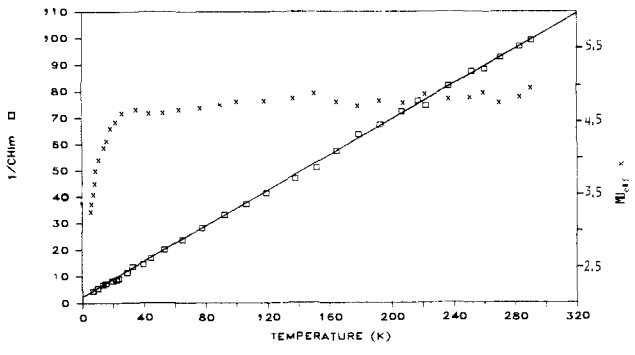

Figure 9. Curie plot (□) of the reciprocal molar susceptibility and μ_{eff} (×) vs. temperature for $[FeCl(TPP\cdot)][SbCl_6]$ (**1**).

counterion. Figure 7 is an ORTEP[39] drawing of the five-coordinate $[FeCl(TpTP\cdot)]^+$ ion showing the atom numbering scheme. A striking feature of this cationic complex is its saddle-shaped conformation. The nearly planar pyrrole rings are tilted alternatively up and down, giving rise to an approximate C_{2v} symmetry to the complex. A similar distortion of the porphyrin core has been found in several other tetraphenylporphyrin cation radical complexes: $Zn(OClO_3)(TPP\cdot)$,[40] $Mg(OClO_3)(TPP\cdot)$,[41] and the dimeric $[Cu(TPP\cdot)][SbCl_6]$.[19]

The individual bond lengths and angles are listed in Tables VI and VII. Bond distances around the iron atom clearly parallel those of FeCl(TPP).[42] The average Fe–N bond length, 2.07 (1) Å, compared to 2.060 (3) Å in FeCl(TPP), falls within the range (2.060–2.087 Å) found for five-coordinate high-spin iron(III) porphyrins,[43] The Fe–Cl distance is 2.168 (5) Å compared to 2,193 (3) Å in FeCl(TPP). The slight contraction is consistent with the increased positive charge on the complex.

The hexachloroantimonate anion is close to octahedral with normal Sb–Cl bond lengths of 2.322 (9)–2.351 (7) Å. Bond lengths of 2.33–2.39 Å are found in hexachloroantimonate structures.[44]

Figure B in the supplementary material shows the atom numbering scheme for the tetrachloroethane molecules. Half of these molecules are on a well-defined site, while the other half are disordered over two sites sharing chlorine TUCl1 with a 0.55/0.45 occupancy ratio.

(38) Mashiko, T.; Kastner, M. E.; Spartalian, K.; Scheidt, W. R.; Reed, C. A. *J. Am. Chem. Soc.* **1978**, *100*, 6354–6362.

(39) Johnson, C. K. *Oak Ridge Natl. Lab., [Rep.] ORNL (U.S.)* **1965**.

(40) Spaulding, L. D.; Eller, P. G.; Bertrand, J. A.; Felton, R. H. *J. Am. Chem. Soc.* **1974**, *96*, 982–987.

(41) Barkigia, K. M.; Spaulding, L. D.; Fajer, J. *Inorg. Chem.* **1983**, *22*, 349–351.

(42) Hoard, J. L.; Cohen, G. H.; Glick, M. D. *J. Am. Chem. Soc.* **1967**, *89*, 1992–1996.

(43) Scheidt, W. R.; Reed, C. A. *Chem. Rev.* **1981**, *81*, 543–555.

(44) (a) Gillespie, R. J.; Kent, J. P.; Sawyer, J. F.; Slim, D. R.; Tyrer, J. D. *Inorg. Chem.* **1981**, *20*, 3799–3812, and references therein. (b) Gillespie, R. J.; Sawyer, J. F.; Slim, D. R.; Tyrer, J. D. *Inorg. Chem.* **1982**, *21*, 1296–1302. (c) Hall, M.; Sowerby, D. B. *J. Chem. Soc., Dalton Trans.* **1983**, *1095*–1099.

Table VII. Bond Angles in the FeCl(TpTP·)$^+$ Cation, $SbCl_6^-$ Anion, and the 1,1,2,2-Tetrachloroethane Solvate Molecules, in deg

N1FeN2	87.4 (5)	C14C15C33	118 (1)
N2FeN3	87.3 (5)	C16C15C33	117 (1)
N3FeN4	87.2 (5)	N4C16C15	122 (1)
N4FeN1	88.0 (5)	N4C16C17	110 (1)
N1FeCl	100.3 (4)	C15C16C17	127 (1)
N2FeCl	102.7 (4)	C18C17C16	108 (1)
N3FeCl	105.5 (4)	C17C18C19	105 (1)
N4FeCl	100.1 (4)	N4C19C20	124 (1)
C1N1C4	107 (1)	N4C19C18	112 (1)
C6N2C9	107 (1)	C20C17C18	124 (1)
C11N3C14	106 (1)	C19C20C1	124 (1)
C16N4C19	105 (1)	C19C20C39	117 (1)
N1C1C20	125 (1)	C1C20C39	119 (1)
N1C1C2	110 (1)	Cl1SbC13	92.2 (2)
C20C1C2	124 (1)	Cl1SbCl4	88.8 (2)
C3C2C1	106 (1)	Cl1SbCl5	92.2 (3)
C2C3C4	107 (1)	Cl1SbCl6	89.4 (2)
N1C4C5	125 (1)	Cl2SbCl3	88.9 (2)
N1C4C3	109 (1)	Cl12SbCl4	88.1 (3)
C5C4C3	126 (1)	C12SbCl5	90.8 (3)
C4C5C6	124 (2)	C12SbCl6	89.3 (2)
C4C5C21	117 (1)	Cl3SbC14	89.5 (3)
C6C5C21	119 (1)	C13SbCl5	92.8 (3)
N2C6C5	126 (1)	Cl4SbCl6	89.8 (3)
N2C6C7	110 (1)	Cl5SbCl6	89.9 (3)
C5C6C7	124 (1)	SC2SC1SCl3	113 (1)
C8C7C6	107 (1)	SC2SC1SCl1	110 (2)
C7C8C9	107 (1)	SCl3SC1SCl1	109 (1)
N2C9C10	124 (1)	SC1SC2SCl2	110 (2)
N2C9C8	109 (1)	SC1SC2SCl4	112 (2)
C10C9C8	126 (1)	SCl2SC2SCl4	110 (1)
C9C10C11	126 (1)	TC2TC1TUCl1	113.9 (2)
C9C10C27	117 (1)	TC2TC1TCl2	110.0 (3)
C11C10C27	117 (7)	TUCl1TC1TCl2	111.6 (4)
N3C11C10	124 (1)	TC1TC2TCl3	107.8 (5)
N3C11C12	110 (1)	TC1TC2TCl4	108.0 (5)
C10C11C12	126 (1)	TC13TC2TCl4	98.0 (8)
C13C12C11	106 (1)	UC2UC1TUCl2	115.1 (2)
C12C13C14	108 (1)	UC2UC1UC12	111.0 (5)
C15C14N3	124 (1)	TUCl1UC1UCl2	117.7 (5)
C15C14C13	126 (1)	UC1UC2UCl4	114.8 (4)
N3C14C13	109 (1)	UC1UC2UCl3	122.6 (4)
C14C15C16	125 (1)	UCl4UC2UCl3	116.0 (5)

Table VIII. Bond Distances (Å) with Standard Deviations in $Fe(OClO_3)_2(TPP\cdot)$

Fe–N1	2.05 (1)	C2–C3	1.39 (3)	C13–C14	1.42 (3)
Fe–N2	2.04 (1)	C3–C4	1.41 (2)	C14–C15	1.40 (3)
Fe–O1	2.13 (1)	C4–C5	1.42 (2)	C15–C16	1.47 (3)
O1–C1	1.54 (1)	C5–C6	1.45 (3)	C16–C11	1.49 (3)
C1–O2	1.40 (1)	C6–C7	1.40 (2)	C10–C17	1.45 (3)
C1–O3	1.42 (2)	C7–C8	1.41 (3)	C17–C18	1.46 (3)
C1–O4	1.41 (2)	C8–C9	1.50 (2)	C18–C19	1.38 (3)
N1–C1	1.34 (2)	C9–C10	1.45 (2)	C19–C20	1.44 (3)
N1–C4	1.41 (2)	C10–C1$_B$	1.44 (2)	C20–C21	1.45 (3)
N2–C6	1.43 (2)	C5–C11	1.56 (2)	C21–C22	1.38 (3)
N2–C9	1.35 (2)	C11–C12	1.34 (3)	C22–C17	1.44 (3)
C1–C2	150 (2)	C12–C13	1.43 (3)		

The crystal lattice of the bis(perchlorato) complex, **2**, is composed of centrosymmetric $Fe(OClO_3)_2(TPP\cdot)$ molecules with a coordination geometry shown in Figure 8. The six-coordinate iron atom is bound to an oxygen atom of both axial perchlorates and to the four nitrogen atoms of the planar macrocycle, and it is required by symmetry to be in the porphyrin plane.

Individual bond lengths and angles are listed in Tables VIII and IX. Bond distances in the coordination unit are consistent with one-electron occupancy of the $d_{x^2-y^2}$ orbital (Fe–N_1 = 2.04 (1) Å; Fe–N_2 = 2.05 (2) Å), and the axial bond distance (Fe–O = 2.13 (1) Å is consistent with the large value of the Mössbauer quadrupole splitting. Bond lengths and angles in the planar porphyrin radical, like those in the saddle-shaped radical, do not show any significant deviation, within experimental error, from those found in six-coordinate or five-coordinate high-spin iron(III) porphyrin complexes.

Table IX. Bond Angles (deg) in the $Fe(OClO_3)_2(TPP\cdot)$ Molecule

N1FeN2	89.8 (5)	C10′C1C2	122 (2)
N1FeO1	89.0 (5)	C5C4C3	124 (2)
N2FeO1	91.7 (5)	C5C6C7	126 (2)
C1N1C4	104 (1)	C10C9C8	122 (2)
C6N2C9	104 (1)	C1C2C3	105 (2)
C4C5C6	128 (2)	C2C3C4	105 (2)
C9C10C1′	123 (2)	C6C7C8	108 (2)
N1C1C10′	127 (2)	C7C8C9	104 (2)
N1C4C5	122 (2)	C4C5C11	116 (2)
N2C6C5	121 (2)	C6C5C11	115 (2)
N2C9C10	125 (2)	C1′C10C17	118 (2)
N1C1C2	111 (2)	C9C10C17	119 (2)
N1C4C3	114 (2)	O1ClO2	109.5 (8)
N2C6C7	112 (2)	O1ClO3	105 (1)
N2C9C8	113 (2)	O1ClO4	109 (1)
FeN1C1	127 (1)	O2ClO3	114 (1)
FeN1C4	129 (1)	O2ClO4	107 (1)
FeN2C6	129 (1)	O3ClO4	113 (1)
FeN2C9	127 (1)	FeO1Cl	131.2 (8)

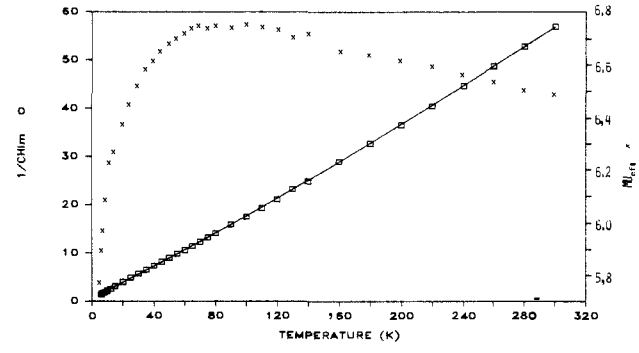

Figure 10. Curie plot (□) of reciprocal molar susceptibility and μ_{eff} (×) vs. temperature for $Fe(OClO_3)_2(TPP\cdot)$ (**2**).

Magnetic Susceptibility. Figure 9 shows the Curie plot for $[FeCl(TPP\cdot)][SbCl_6]$ (**1**). The solid line is a linear least-squares fit which extrapolates to θ = −7.5 K. The magnitude of the suceptibility and the linearity of the data imply strong antiferromagnetic coupling of the $S = {}^5/_2$ iron atom to the $S = {}^1/_2$ porphyrin radical to give an overall S = 2 state. The lack of downward curvature of the data at high temperatures indicates that a higher multiplicity state is not thermally accessible. This places the S = 3 state > 1500 cm^{-1} above the S = 2 state and corresponds to a $2J$ value of −500 cm^{-1}. An error of 3% in the room-temperature susceptibility would mean a lower limit of $|-2J|$ > 250 cm^{-1}, but this may be an unduly pessimistic estimate of our ability to detect curvature. Figure 9 also shows the μ_{eff} vs. T plot for **1**. The room temperature moment is 4.80 μ_B, which is within experimental error of the spin-only value (4.90 μ_B). An ESR signal was not observed for **1** either in frozen dichloromethane solutions or in solid microcrystalline form, at temperatures down to 77 K.

Figure 10 shows a plot of μ_{eff} vs. T for $Fe(OClO_3)_2(TPP\cdot)$ (**2**). The room temperature moment of 6.50 μ_B lies between the spin-only values of 6.93 and 4.90 μ_B for S = 3 and S = 2 systems, respectively. It is also greater than the spin-only value for an uncoupled $S = {}^5/_2$, $S = {}^1/_2$ system (6.17 μ_B). The *increase* of μ_{eff} as the temperature decreases to 100 K indicates that the state of highest multiplicity is lowest in energy. A maximum value of about 6.75 μ_B is reached near 100 K, and the extrapolation of the linear portion of the data to 0 K gives a μ_{eff} value of about 6.9 μ_B, indicating an S = 3 ground state. This implies ferromagnetic coupling of the $S = {}^5/_2$ iron to the $S = {}^1/_2$ porphyrin radical. The rapid decrease of μ_{eff} below 50 K is expected from zero-field splitting effects, and a theoretical fit to these data along with detailed Mössbauer studies is the subject of a separate publication.[45] Figure 10 also shows the Curie plot for **2**. Extrapolation of the linear low-temperature portion of the data leads to θ = −2.8

(45) Lang, G.; Boso, B.; Erler, B. S.; Reed, C. A. *J. Chem. Phys.*, in press.

K. The solid line in Figure 10 is a theoretical fit to a spin Hamiltonian with $2J = +78$ cm^{-1} and $g = 1.98$. This places the $S = 2$ state some 234 cm^{-1} above the $S = 3$ ground state. A realistic estimate of the error limits for the determination of this energy gap and its $2J$ value is ±20%. ESR spectra, recorded on frozen solutions of **2** in dichloromethane between 4.2 and 110 K, failed to show an ESR signal that could be assigned to this species.

Discussion

Synthesis. While electrochemical methods are very convenient for the in situ generation of oxidized metalloporphyrins, the characterization of products is usually limited to solution spectroscopic techniques. The isolation of analytically pure materials is rarely achieved, chiefly because of the difficulty of removing large molar excesses of electrolyte. Poor volatility of the high-dielectric solvents frequently required for electrochemistry is another common problem, although the use of dichloromethane in work with iron porphyrin oxidation does avoid this aspect of the problem. We sought a synthetic method which retained the advantage of a rather precisely determined electrochemical oxidation potential but which was synthetically clean and convenient. The idea was to find a stable organic radical cation salt, $(R^{+}\cdot)Y^{-}$, whose $R/R^{+}\cdot$ redox couple matched that of the required metalloporphyrin redox reaction. A range of such redox reagents would represent the synthetic equivalent of controlled potential electrolysis. Ideally, a simple stoichiometric reaction would occur (eq 1). The choice of $R^{+}\cdot$ should be such that the reduction product

$$(R^{+}\cdot)Y^{-} + M(TPP) \rightarrow M(TPP)^{+}Y^{-} + R \qquad (1)$$

R is nonligating and noninterfering. It should be easily separated from the desired product preferably by remaining soluble in the supernatant after the product has crystallized out. A range of anions Y^{-} would provide synthetic flexibility, and weakly coordinating, relatively inert ions such as ClO_4^{-}, PF_6^{-}, and $SbCl_6^{-}$ were deemed to be most useful.

We find that phenoxathiin and thianthrene are both convenient for this purpose. Their radical cations are readily synthesized and isolated as perchlorate, hexachloroantimonate, or hexafluoroantimonate salts. They can be weighed out for stoichiometric use, and moreover, since the cations $R^{+}\cdot$ are intensely blue but the neutral R is colorless, they are titratable. They appear to be nonligating in the present circumstances, although we sometimes find their trace inclusion in the initially isolated metalloporphyrin products. A report on the scope of their utility with metalloporphyrins other than iron will appear elsewhere.[46] The $R/R^{+}\cdot$ redox potentials of phenoxathiin and thianthrene are 1.20 and 1.22 V, respectively, in CH_2Cl_2 relative to SCE. The oxidation potentials for FeCl(TPP) and $Fe(OClO_3)$(TPP) are 1.03 and 1.04 V under the same conditions, so that both redox reagents are appropriately matched for both oxidations. The final choice of phenoxathiinylium hexachloroantimonate, $(Phox^{+}\cdot)SbCl_6^{-}$, for the oxidation of FeCl(TPP) (eq 2) and of FeCl(OEP) and thian-

$$FeCl(TPP) + (Phox^{+}\cdot)SbCl_6^{-} \xrightarrow{CH_2Cl_2} [FeCl(TPP\cdot)][SbCl_6]\ (\mathbf{1}) + Phox \qquad (2)$$

$$Fe(OClO_3)(TPP) + (Thian^{+}\cdot)ClO_4^{-} \xrightarrow{CH_2Cl_2} Fe(OClO_3)_2(TPP\cdot)\ (\mathbf{2}) + Thian \qquad (3)$$

threnium perchlorate, $(Thian^{+}\cdot)ClO_4^{-}$, for the oxidation of $Fe(OClO_3)$(TPP) was based on the ease with which crystalline, analytically pure products could be obtained. Solvent choice for these reactions is largely limited to halogenated hydrocarbons, since nucleophilic solvents react with both the $R^{+}\cdot$ reagents and the porphyrin radical cation products. Inclusion of molecules of solvation in stoichiometric and nonstoichiometric amounts was commonly observed.

An alternative method of synthesis for $Fe(OClO_3)_2(TPP\cdot)$ was developed by using ferric perchlorate as the oxidant. An independent synthetic method was necessary for the magnetic work on this compound. Absolute values of the susceptibility became very important (vide infra), and contamination by paramagnetic impurities had to be ruled out. Analytically pure materials were obtained by both methods, and repeated magnetic susceptibility measurements on different preparations showed reproducibility within 5%.

Electronic Spectra. Early work on the oxidation of metalloporphyrins relied heavily on UV–vis spectroscopy to decide whether oxidation was metal-centered or ring-centered. This was done because of the convenience of the method and also because the distinction between a metalloporphyrin-type spectrum and a metalloporphyrin π-radical-cation-type spectrum was shown to be very clear in the case of non-redox active metals such as zinc or magnesium.[29] The characteristics of a radical cation species are typically a broadened α,β region, a new band at low energy, and a dramatically broadened, low-intensity, blue-shifted Soret band relative to the unoxidized species. It was probably with this expectation that the much less dramatic spectral changes upon oxidation of FeCl(TPP) to $[FeCl(TPP\cdot)]^{+}$ were not immediately taken as diagnostic of ring oxidation.[10] The point is made even more strongly by the spectral comparison of $Fe(OClO_3)$(TPP) and $Fe(OClO_3)_2(TPP\cdot)$ in Figure 1. Although most of the features of a radical spectrum are present, we note that the Soret intensity is in fact slightly increased from that of the parent compound, which has a "normal" Soret intensity. These results suggest that caution be used in relying upon UV–vis spectroscopy as the sole criterion of the site of oxidation. Other candidates for reformulation are the oxidized cobalt(II) porphyrins,[19] but these will be the subject of a future publication.[46]

One curious feature of the α,β-region spectra of tolyl analogues of **1** and **2** illustrated in Figure 2 is the sensitivity of this region to the ortho, meta, or para position of the methyl substituent. This probably reflects an enhanced sensitivity to charge delocalization patterns in the radical and suggests a possible new criterion for ring oxidation, at least for an a_{2u}-type radical cation where unpaired electron density is localized in close proximity to the phenyl groups on the methine carbon atoms. The optical spectra of **1** and **2** show features which are more characteristic of certain a_{2u}-type radicals[10] than a_{1u}-type radicals, and this leads us to favor an a_{2u} description for the porphyrin half-occupied HOMO's. NMR spectra also support this assignment (vide infra).

Infrared Spectra. The observation[30] that a strongly infrared active mode at about 1290 cm^{-1} is diagnostic of the tetraphenylporphyrin π-cation radical is proving to be a very useful criterion for or against ring oxidation.[12d,47] A precise description of the mode is not yet available, but it is known to be sensitive to both pyrrole and phenyl deuteration.[30] In octaethylporphyrin complexes such as $[FeCl(OEP\cdot)][SbCl_6]$ an apparently analogous band appears strongly in the infrared spectrum at about 1535 cm^{-1}. This is illustrated in Figure 3 by comparison to the starting material FeCl(OEP).

Electrochemistry. It has been pointed out that the near constancy of the redox potential for the $FeX(TPP)^{0/+}$ couple as a function of different axial ligands X^{-} is a good indication of ring oxidation rather than iron oxidation.[11b] Our electrochemical results support this conclusion. As well, they show that $Fe(OClO_3)_2$(TPP·) can be produced from the water-containing species $[Fe(H_2O)_2(TPP)]^{+}$, and they establish that a single-electron oxidation process takes place.

NMR Spectra. The three aforementioned physical probes of the oxidized species (UV–vis, IR, E^0) focus on the oxidation state of the porphyrin ligand rather than the metal atom. And while NMR spectroscopy does probe the environment of protons at the extreme periphery of the ligand, the chemical shifts of these protons are stongly influenced by the spin state of the metal atom. The following discussion assumes that a high-spin iron(III) exists in both **1** and **2**, an assertion that will be justified during our discussion of the physical methods that specifically probe the state

(46) Erler, B. S.; Scheidt, W. R.; Reed, C. A. to be submitted.

(47) Camenzind, M. J.; Hollander, F. J.; Hill, C. L. *Inorg. Chem.* **1983**, *22*, 3776–3784.

of the iron: Mössbauer, X-ray, and magnetism.

Extensive studies by Goff and co-workers[11d] have led to two major generalizations for oxidized iron porphyrins. Firstly, there are large paramagnetic shifts of the phenyl protons in π-cation-radical complexes, Distinctively, the ortho and para protons are shifted in the opposite direction to the meta (see Table IV). We notice also the curious feature that the direction of these shifts is completely reversed between **1** and **2**. The downfield ortho, para protons (42, 35 ppm) and upfield, meta protons (−12 ppm) in $[FeCl(TPP\cdot)]^+$ contrast sharply with the *upfield* ortho, para protons (−19, −13 ppm) and downfield meta protons (35 ppm) in $Fe(OClO_3)_2(TPP\cdot)$. This feature can be understood as the result of a spin flip in the porphyrin radical moiety. There is a different type of magnetic coupling in these two species, antiferromagnetic in **1** and ferromagnetic in **2** (vide infra). This means that the natural atom by atom alternation of spin inherent to a π spin delocalization mechanism[48] is reversed on going from **1** to **2**.

Secondly, the pyrrole protons are particularly sensitive to the spin state of the iron atom; a large downfield shift is associated with unpaired spin in the $d_{x^2-y^2}$ orbital. Thus, high-spin iron(III) complexes such as FeCl(TPP) have pyrrole resonances near 80 ppm downfield of Me_4Si. The observed 69 ppm downfield shift in $[FeCl(TPP\cdot)]^+$ and the 31 ppm downfield shift in $Fe(OClO_3)_2(TPP\cdot)$ are taken to indicate that the presence of the radical spin can significantly moderate the effect of $d_{x^2-y^2}$ occupation, Goff[11d] has interpreted the difference in the pyrrole shift between **1** and **2** as resulting from the effect of $S = {}^3/_2, {}^5/_2$ spin admixture in the latter. While this explanation is quite plausible, an alternative is suggested by our solid-state measurements (vide infra), which characterize the spin state of iron in **2** as high spin rather than admixed intermediate, These measurements show that the radical spin is *ferro*magnetically coupled to the iron, leading to an $S = 3$ ground state. The coupling constant $2J$, however, is of moderate magnitude ($\sim$80 cm^{-1}), and this leads to an energy gap separation of $\sim$250 cm^{-1} between the $S = 3$ and $S = 2$ levels. Thus, at room temperature there is significant thermal population of both states, and a temperature-dependent NMR spectrum is expected. Deviation from Curie law behavior of the chemical shifts is also expected. This is, in fact, observed.[11d] Thus, the smaller downfield shift of the pyrrole protons in the bis(perchlorato) species compared to the oxidized chloro complex does not require that the admixed $S = {}^3/_2, {}^5/_2$ character of $Fe(OClO_3)(TPP)$[24] be preserved upon oxidation. To our knowledge no significant $S = {}^3/_2, {}^5/_2$ admixed character has been shown in any six-coordinate iron(III) TPP species, although it is possible that the solution species differs from that in the solid state. Given that the solid-state properties provide an equally plausible explanation for the attenuation of the downfield pyrrole shifts in **2**, we presently adopt the idea that *ferro*magnetic coupling of porphyrin radical spin to high-spin iron is responsible rather than spin admixture. The same explanation can apply to the recently reported tetramesitylporphyrin analogue, which also shows a nonlinear Curie plot for the pyrrole chemical shift.[12d] On the other hand, *antiferro*magnetic coupling in $[FeCl(TPP\cdot)]^+$ apparently modulates the large downfield shift of FeCl(TPP) to a much smaller degree.

Finally, the NMR spectra of **1** and **2** lend support to an a_{2u} assignment for the radical type in both **1** and **2**.[11c,d] The concentration of spin density at the methine carbon atoms (a_{2u}) rather than the pyrrole carbon atoms (a_{1u}) provides an explanation for the large shifts seen for the ortho, meta, and para protons. We note that the familiar a_{2u} designation is a label of convenience used to indicate the predominant character of the radical. Strictly speaking, it should be applied only in molecules of D_{4h} symmetry.

Mössbauer Spectroscopy. It is now widely recognized that Mössbauer spectroscopy is one of the most useful and most direct probes of the oxidation state of the iron in iron porphyrins and hemoproteins.[34,35,49] Simple isomer shift (δ) and quadrupole splitting (ΔE_Q) data measured in zero applied magnetic field are usually sufficient to identify both the oxidation state and the spin state. It is of interest to explore whether this remains true when the iron spin state is perturbed by the close proximity of a ligand radical.

That the Mössbauer data for **1** are almost identical with those of the parent compound FeCl(TPP) (Table V) is compelling evidence that oxidation has occurred at the porphyrin ring in a site remote from the iron atom.[17] An infrared integrity check monitoring the diagnostic 1290-cm^{-1} band following collection of the Mössbauer data showed that photoreduction by the γ-ray beam was not occurring. The Mössbauer data for **2** are equally diagnostic of a high-spin iron(III) state, but comparison is not made to its parent compound $Fe(OClO_3)(TPP)$ because this species has an admixed $S = {}^3/_2, {}^5/_2$ spin state.[24] Instead, comparison is made in Table V to structurally related six-coordinate high-spin iron(III) complexes with oxygen donor atoms as axial ligands. Although isomer shift values do not distinguish between high-spin and admixed intermediate-spin states, quadrupole splitting values do. Characteristically large ΔE_Q values (ca. 3 mm s^{-1}) are observed for significantly admixed intermediate-spin states. However, the ΔE_Q value for **2** is moderate in magnitude and falls in the range typical of six-coordinate high-spin iron(III) porphyrins.[36-38]

The isomer shift values of both **1** and **2** are clearly quite unlike those of any iron(IV) porphyrins or iron(IV) hemoproteins where low values in the range 0.0–0.11 are observed. The effect of the porphyrin radical on the Mössbauer spectra of the iron atom is seen to be minimal under the conditions used in the present experiments. This observation may be generally true, and it rationalizes the fact that horseradish peroxidase compounds I and II, which are described as iron(IV) porphyrin cation radical and iron(IV) porphyrin species, respectively, have very similar zero-field Mössbauer parameters.[5] This has also been confirmed in model studies.[50]

We do find, however, that when data are collected in the presence of applied magnetic fields there are greater differences in the hyperfine structure between parent and oxidized species. There studies are the subject of a separate publication.[45] They are of particular interest because hemoproteins such as cytochrome oxidase[51] and sulfite reductase[52] also have high-spin iron(III) hemes that are strongly magnetically coupled to nearby spins.

Magnetism. When an $S = {}^1/_2$ porphyrin radical moiety is coordinated to an $S = {}^5/_2$ high-spin iron(III) center there are three possible descriptions of the overall spin state. Firstly, *antiferromagnetic coupling* would lead to an $S = 2$ ground state. If the magnitude of the coupling constant ($-2J$) is several hundred wavenumbers, then there would be no population of the higher multiplicity $S = 3$ state at room temperature. Simple Curie–Weiss law magnetic data consistent with four unpaired electrons (spin only $\mu_{eff}^{300K} = 4,9\ \mu_B$) would be expected. As we shall see, this is the case for **1**. Secondly, *ferromagnetic coupling* would lead to an $S = 3$ ground state. A spin-only magnetic moment of 6.9 μ_B would be expected if the magnitude of the coupling constant ($+2J$) is very large. Smaller values of $2J$ would lead to thermal population of the lower multiplicity $S = 2$ state at high temperatures. Lower magnetic moments and curvature of the Curie plot would result. Thirdly, if the iron spin was *noninteracting* with the porphyrin spin, then the $S = {}^5/_2$, $S = {}^1/_2$ spin system would be expected to show magnetic moments given by the square root of the sum of the squares of the individual moments. The spin-only value at 25 °C would be 6.17 μ_B. Our initial data showed that this state had to be considered as a possible candidate for the spin description of **2**, but we now present additional data that allow us to rule out this possibility for any of the present compounds. Such a description, however, is very nearly the case for HRP I.

(48) Horrocks, W. DeW. "NMR of Paramagnetic Compounds"; La Mar, G. N.; Horrocks, W. DeW; Holm, R. H., Eds.; Academic: New York, 1973, Chapter 4.

(49) English, D. R.; Hendrikson, D. N.; Suslick, K. S. *Inorg. Chem.* **1983**, *22*, 367–368.

(50) Boso, B.; Lang, G.; McMurry, T. J.; Groves, J. T. *J. Chem. Phys.* **1983**, *79*, 1122–1126.

(51) Kent, T. A.; Young, L. J.; Palmer, G.; Fee, J. A.; Munck, E. *J. Biol. Chem.* **1983**, *258*, 8543–8546.

(52) Chistner, J. A.; Munck, E.; Kent, T. A.; Janick, P. A.; Salerno, J. C.; Siegel, L. M. *J. Am. Chem. Soc.* **1984**, *106*, 6786–6794.

The magnetic susceptibility data for microcrystalline **1** are straightforwardly interpreted in terms of an $S = 2$ state. This is consistent with conclusions based on solution magnetic moments.[10,11] Since the X-ray and Mössbauer data show unambiguously that the iron atom is in a high-spin state, strong antiferromagnetic coupling between the $S = {}^5/_2$ iron and the $S = {}^1/_2$ radical must exist. A very conservative estimate of the energy gap between the $S = 2$ and $S = 3$ levels is 750 cm^{-1}, but it is probably >1500 cm^{-1}. By marked contrast, the magnetic susceptibility data for **2** are fit to an $S = 3$ ferromagnetically coupled ground state. The $S = 2$ level is approximately 230 cm^{-1} higher in energy. An explanation for the *antiferro*magnetism of **1** vs. the *ferro*magnetism of **2** can be found in the different symmetries of their structures. We begin our discussion with the more symmetrical complex **2**, $Fe(OClO_3)_2(TPP\cdot)$.

The crystal structure of **2** reveals a planar porphyrin core, symmetrical axial ligation, and the iron atom sitting at the center of symmetry (Figure 8). This imposes effective D_{4h} symmetry upon the iron atom, and in this point group the five half-filled d orbitals (x^2-y^2, z^2, xz, yz, xy) have b_{1g}, a_{1g}, e_g, e_g, and b_{2g} symmetry. Since the half-filled porphyrin a_{2u} orbital has different symmetry from all of the d orbitals we see that all six magnetic orbitals[53] are strictly orthogonal. Provided that all spins know about each other, this means that the lowest energy state of the molecule must be an $S = 3$ state with all spins parallel. In essence, this is an application of Hund's rule of maximum multiplicity. In the language of molecular orbital theory there is no net overlap of the ligand orbital with the metal orbitals, and the $S = 3$ state is a manifestation of the exchange energy term in the wavefunction. Indeed, the $+2J$ value of $\sim$80 cm^{-1} must be directly related to its magnitude. The language of the spin Hamiltonian treatment of the magnetic data leads to an equivalent description of the ground state as *ferro*magnetic coupling of the ligand and metal spins.

The crystal structure of **3**, on the other hand, reveals a saddle-shaped porphyrin core, unsymmetrical axial ligation, and the iron atom sitting at a site of approximate C_{2v} symmetry. We assume that the same is true for **1** since the spectroscopic properties of **1** and **3** are entirely compatible. Upon such lowering of the iron site symmetry from D_{4h} to C_{2v} the d orbital symmetries reduce to a_1, a_1, b_1, b_2, and a_2. The porphyrin a_{2u} orbital symmetry reduces to a_1, and we see that overlap of this ligand orbital with two of the metal orbitals becomes symmetry allowed. In the language of molecular orbital theory there is overlap of the ligand a_1 symmetry orbital with a metal a_1 symmetry orbital to give a bonding molecular orbital of lower energy and an antibonding molecular orbital of higher energy. Electron occupation will, of course, lead to spin-pairing in the lower state, giving the molecule an overall $S = 2$ ground state. On the other hand, the language of the spin Hamiltonian treatment leads to an equivalent description in terms of an *antiferro*magnetically coupled ground state. We should add that although the description of antiferromagnetism in terms of molecular orbital overlap requires the formation of a bond, this bond may be extremely weak. Indeed, the $2J$ value of 500 cm^{-1} translates into an energy of <2 kcal.

Orbital overlap terms quickly dominate exchange terms in molecular orbital theory once a system is removed from strict orthogonality of its atomic orbitals. It is not surprising, therefore, to find that the antiferromagnetic coupling in **1** is much stronger than the ferromagnetic coupling in **2**. However, the ferromagnetism in **2** ($2J \sim 80$ cm^{-1}) is quite large by the benchmark of binuclear complexes.[54] It will be interesting to find out how this varies with the nature of the metal and its spin state and with the nature of the ligand orbital (a_{1u} and a_{2u} character). It will also be interesting to find out how much distortion from D_{4h} symmetry is required for antiferromangetic coupling to dominate over ferromagnetic coupling. The literature data on HRP I and a related model compound are suggestive of an answer to this question. The model compound $Fe^{IV}(O)Cl(TMP\cdot)$ (TMP· = radical cation of *meso*-tetramesitylporphyrin) has been analyzed by Mössbauer spectroscopy to have an $S = {}^3/_2$ ground state.[50] No indication of a state of lower multiplicity was observed in data collected up to 60 K. This probably places a lower limit of about 60 cm^{-1} on the magnitude of $2J$. Such ferromagnetic coupling between the $S = 1$ iron(IV) and the $S = {}^1/_2$ porphyrin radical is expected if a high degree of symmetry is retained in this complex. C_{2v} symmetry would be sufficient to preserve orthogonality of the metal and ligand orbitals. In C_{2v} symmetry the xz and yz magnetic orbitals of the $S = 1$ iron(IV) would have b_1 and b_2 symmetry and the a_{2u}-type porphyrin radical would have a_1 symmetry. The lack of z^2 or x^2-y^2 occupation clearly reduces greatly the opportunity for antiferromagnetism. On the other hand, the analogous protein species HRP I has been analyzed in terms of a very weakly coupled system having $2J$ about -2 cm^{-1}.[20] We can understand this difference between the model complex and the protein as arising from the lower symmetry of the protein. The axial histidine, the peripheral heme substituents, and the asymmetric protein wrapping of the heme group must all conspire to remove the iron atom from an environment of strict symmetry. It is quite possible that by a fortuitous accident the distortion is just enough to balance the opposing effects of overlap and exchange (or antiferromagnetism and ferromagnetism), and an essentially noninteracting system results.

A possibly related case is that of a ruthenium(III) porphyrin radical cation species[55] where EPR signals from the $S = {}^1/_2$ ruthenium and the $S = {}^1/_2$ porphyrin are reported to be virtually unperturbed by their proximity, at least at 77 K.

Another related case is that of the low-spin bis(imidazole)-iron(III) porphyrin radical cation $[Fe(Im)_2(TPP\cdot)]^{2+}$. Its magnetic properties have been interpreted in terms of a pair of noninteracting $S = {}^1/_2$ spins.[56] However, in the light of the understanding of magnetic interactions gained from the present study this system is more readily interpreted in terms of an $S = 1$ ferromagnet. The experimentally determined magnetic moment of 2.8 ± 0.2 μ_B is in fact equal to the spin-only value for an $S = 1$ system (2.83 μ_B) rather than the spin-only value for noninteracting spins (2.45 μ_B). The lack of an EPR signal is consistent with an integral spin state. But perhaps the most suggestive evidence for ferromagnetic coupling is the sign of the ortho, para, and meta phenyl resonances in the ^1H NMR spectrum. They follow the same pattern as the ferromagnet **2** (ortho, para upfield, meta downfield) but are reversed from those of the antiferromagnet **1**. In fact, it is apparent now that all axially symmetric iron porphyrin radical cations, where ferromagnetism is to be expected from orthogonality of the magnetic orbitals, show the same pattern. For example, iron(IV) radical species $Fe(O)(TPP\cdot)Cl$[12c] shows upfield ortho, para resonances and downfield meta resonances. By comparison to the mesitylporphyrin analogue discussed earlier this system almost certainly has an $S = {}^3/_2$ ground state arising from ferromagnetic coupling of the $S = 1$ and $S = {}^1/_2$ spins. Interestingly, when methyl groups replace the ortho and para protons in mesitylporphyrin derivatives the methyl protons have the opposite sign to the aryl protons. Thus, all the phenyl and methyl resonances are downfield in $Fe(OClO_3)_2(TMP\cdot)$.[12d,14f] Atom to atom alternation of nuclear spin is an expected result of a π-delocalization,[48] and we can now understand the noted correlation of shift patterns[12d,14f,56] with the type of magnetic coupling. It may prove to be a general observation in metalloporphyrin radical cations that ferromagnetic coupling with a metal spin gives rise to upfield ortho, para resonances and downfield meta resonances in TPP derivatives. Likewise, downfield ortho, para resonances and upfield meta resonances may be a general signature of antiferromagnetic coupling in TPP derivatives.

We are presently exploring the scope and generality of the symmetry-based rationale for ferro- vs. antiferromagnetism in

(53) The term *magnetic orbital* has been coined to refer to an orbital containing an unpaired electron: Kahn, O. *Inorg. Chim. Acta.* **1982**, *62*, 3–14.
(54) Kahn, O. *Comments Inorg. Chem.* **1984**, *3*, 105–132.
(55) Barley, M.; Becker, J. Y.; Domazetis, G.; Dolphin, D.; James, B. R. *Can. J. Chem.* **1983**, *61*, 2389–2396.
(56) Goff, H. M.; Phillippi, M. A. *J. Am. Chem. Soc.* **1983**, *105*, 7567–7571.

metalloporphyrin radicals of Cu, V, Cr, and Mn. For example, $[Cu(TPP\cdot)]^+$ is diamagnetic in the solid state, and its structure is highly distorted from D_{4h} symmetry.[19] Antiferromagnetic coupling to give an $S = 0$ state is expected by analogy to **1**. On the other hand, $[Cu(TMP\cdot)]^+$, whose mesityl groups presumably prevent dimer formation and accompanying distortion from D_{4h} symmetry, is an $S = 1$ ferromagnet.[46]

Conclusion

It is apparent from this fairly exhaustive probing of the nature of $[FeCl(TPP\cdot)]^+$ and $Fe(OClO_3)_2(TPP\cdot)$ that these species are oxidized at the porphyrin ring and are not iron(IV) complexes. The UV-vis absorption features are seen now to be characteristic of π-cation radicals, but not dramatically so. The most definitive criteria for making the correct assignment of the site of oxidation have turned out to be Mössbauer spectroscopy, X-ray structure, NMR spectroscopy, and, most simply, IR spectroscopy. Electrochemical and magnetic susceptibility criteria are also useful in favorable circumstances.

The present compounds illustrate a theme in coordination chemistry that is becoming increasingly familiar. We note that axial ligation by chloride or perchlorate leads to iron(III) porphyrins that are oxidized at the porphyrin ring. On the other hand, the presence of terminal oxide[14] or methoxide[12d] ligation leads to authentic iron(IV) porphyrins. Thus, the site of redox is seen to be largely dictated by the nature of the axial ligation. The excellent $2_{p\pi}$ donor properties of terminal oxo and alkoxo ligands probably provides the best explanation for the ability of these ligands (along with carbido, nitrido,[49] and fluoro[57]) to stabilize high oxidation states of metals.

Perhaps the most unexpected feature of interest to come out of this work has been the clear distinction between antiferromagnetic and ferromagnetic coupling of the metal and ligand spins in $[FeCl(TPP\cdot)]^+$ and $Fe(OClO_3)_2(TPP\cdot)$. The magnetostructural correlation in terms of the symmetries of the magnetic orbitals can be described with heuristically appealing simplicity and may have wide generality.

Acknowledgment. We thank Michael Verdaguer for fruitful discussions. Work at the University of Southern California was supported by the National Science Foundation (CHE 8026812). Support of the CNRS (UA321: Chimie et Physicochimie Moleculaires) for work at the Centre d'Etudes Nucleaires de Grenoble is gratefully acknowledged.

Supplementary Material Available: Structure factor tables and thermal parameters (Tables A and B) and Figures A and B (4 pages) of proton chemical shifts and an atom numbering scheme (42 pages). Ordering information can be found on any current masthead page.

(57) Hickman, D. L.; Goff, H. M. *Inorg. Chem.* **1983**, *22*, 2787-2789.

Role of the Acetylacetonyl Radical in the Sensitized Photoreduction of Bis(acetylacetonato)copper(II)

Yuan L. Chow* and Gonzalo E. Buono-Core

Contribution from the Department of Chemistry, Simon Fraser University, Burnaby, British Columbia, Canada V5A 1S6. *Received August 5, 1985*

Abstract: Benzophenone-sensitized photoreduction of $Cu(acac)_2$ generated the acetylacetonyl radical (acac·) which could be trapped as acetylacetone by hydrogen as well as by a H-atom-donating agent, or as the corresponding nitroxide with 2-nitroso-2-methylpropane, or as addition products with some simple olefins. Observations indicate that the photoreduction to Cu(acac) occurs only if the acetylacetonyl radical is rapidly scavenged so that the reverse electron transfer cannot compete with the trapping process. The acetylacetonyl radical was found to abstract a hydrogen atom as well as to add to the double bond of olefins and behave primarily as a C radical in addition reactions. The relative importance of oxidation of radicals by copper(II) salt was shown to be dependent on their structures.

We have discovered[2-4] that the triplet excited state of aryl ketones sensitized the photoreduction of bis(acetylacetonato)-copper(II), $Cu(acac)_2$, to (acetylacetonato)copper(I), Cu(acac), in an H-atom-donating solvent (SH). The solvent was concomitantly oxidized. The fast interaction of a triplet excited ketone with $Cu(acac)_2$ ($k_q = 10^{10} \approx 10^9$ M^{-1} s^{-1}) was assumed to involve charge transfer as well as spin-exchange processes within complexes leading to the generation of an acetylacetonyl radical from an oxidized species[3] of $Cu(acac)_2$ (eq 1). The association com-

$$Cu(acac)_2 + {}^*Ph_2CO \rightarrow \underset{\mathbf{1}}{[Cu(acac)_2^+\cdot\cdot\cdot Ph_2CO^-\cdot]} \rightarrow \underset{\mathbf{2}}{[Cu(acac)^+\cdot\cdot\cdot Ph_2CO^-\cdot\cdot\cdot acac\cdot]} \quad (1)$$

$$Cu(acac)^+ + Ph_2CO^-\cdot \rightarrow Cu(acac) + Ph_2CO \quad (2)$$

$$acac\cdot + SH \rightarrow acacH + S\cdot \quad (3)$$

$$Cu(acac)^+ + Ph_2CO^-\cdot + acac\cdot \rightarrow Cu(acac)_2 + Ph_2CO \quad (4)$$

plexes **1** and **2** have been assumed for the convenience of kinetic analysis. The reactions of each components are formally shown in eq 2-4 without indicating the degree of association. Since the quantum efficiency of the sensitized photoreduction follows the order of the hydrogen-donating power of solvents, e.g., *i*-PrOH > EtOH > MeOH $\gg$ C_6H_6 (no reaction in benzene),[2,3] eq 3 is the rate-determining step. Therefore, the occurrence of photoreduction depends on a favorable competition of H-abstraction

(1) A part of the results were published as a communication; see: Chow, Y. L.; Buono-Core, G. E. *J. Am. Chem. Soc.* **1982**, *104*, 3770.
(2) Chow, Y. L.; Buono-Core, G. E. *Can. J. Chem.* **1983**, *61*, 795.
(3) Chow, Y. L.; Buono-Core, G. E.; Marciniak, B.; Beddard, C. *Can. J. Chem.* **1983**, *61*, 801.
(4) Chow, Y. L.; Buono-Core, G. E.; Marciniak, B.; Li, H. L. *J. Chem. Soc. Perkin Trans. 2*, in press.

0002-7863/86/1508-1234$01.50/0